$(TTiPP^+)Rh(I)_2^-$. This compound was then washed twice with a sodium thiosulfate solution for removal of excess iodine and then with water. The final product (TTiPP)RhI, was then dissolved in chloroform and dried with anhydrous $MgSO_4$.

(TTiPP)Rh•. Photolysis of $(TTiPP)RhCH_3$ in benzene produced the metalloradical, (TTiPP)Rh•, at ambient temperature. Clean conversion of $(TTiPP)RhCH_3$ to the metallo radical species was obtained by irradiation of 1-mg samples of $(TTiPP)RhCH_3$ in 0.5 mL of benzene for ~6 h ($\lambda \geq 350$ nm):

$$2(TTiPP)RhCH_3 + C_6D_6 \rightarrow 2(TTiPP)Rh^\bullet + CH_3D + C_6D_5CH_3$$

^1H NMR (C_6D_6, 298 K) δ 18.4 (broad, 8 H, pyrrole H), 9.19 (broad, 8 H, arom), 4.19 (broad, 12 H, $-CH(CH_3)_2$), 2.38 (broad, 24 H, $-CH(CH_3)_2$), 1.53 (broad, 48 H, $-CH(CH_3)_2$).

(TTiPP)RhCO. Exposure of NMR samples containing (TTiPP)Rh• in benzene or toluene to carbon monoxide ($P_{CO} > 100$ Torr) resulted in the formation of (TTiPP)RhCO. The ^1H NMR spectrum for (TTiPP)RhCO displays broad contact shifted resonances at room temperature. No diamagnetic products were observed: ^1H NMR (C_6D_6, 298 K, 450 Torr of CO) δ 18.0 (broad, 8 H, pyrrole H), 9.15 (broad, 8 H, arom), 4.05 (broad, 12 H, $-CH(CH_3)_2$), 2.254 (broad, 24 H, $-CH(CH_3)_2$), 1.50 (broad, 48 H, $-CH(CH_3)_2$).

Addition of ^{13}CO to a toluene solution of (TTiPP)Rh• produced $(TTiPP)Rh^{13}CO$ which displays an isotropic EPR spectrum ($\langle g \rangle = 2.10$, $\langle A(^{13}C) \rangle = 320$ MHz). Frozen toluene solutions (90 K) display three distinct g values and ^{13}C coupling constants associated with a nonlinear RhCO unit ($g_1 = 2.167$; $g_2 = 2.130$; $g_3 = 2.000$; $A(^{13}C_{(g_1)}) = 318$ MHz; $A(^{13}C_{(g_2)}) = 347$ MHz; $A(^{13}C_{(g_3)}) = 305$ MHz; $A(^{13}C_{(g_3)}) = 65$ MHz). In contrast with (TMP)RhCO, lowering the temperature from 283 to 233 K resulted in a regular increase in the intensity of the isotropic EPR of (TTiPP)RhCO.

Acknowledgment. This work was supported by the National Science Foundation and the Department of Energy, Division of Chemical Sciences, Office of Basic Energy Sciences, Grant DE-FG02-86ER13615.

Spin Exchange Coupling in Asymmetric Heterodinuclear Complexes Containing the μ-Oxo-bis(μ-acetato)dimetal Core

Rainer Hotzelmann,[1a] Karl Wieghardt,*[,1a] Ulrich Flörke,[1b] Hans-Jürgen Haupt,[1b] David C. Weatherburn,[1c] Jacques Bonvoisin,[‡,1d] Geneviève Blondin,[1d] and Jean-Jacques Girerd*[,1d]

Contribution from the Lehrstuhl für Anorganische Chemie I, Ruhr-Universität, D-4630 Bochum, FRG, the Lehrstuhl für Allgemeine Anorganische und Analytische Chemie der Universität-Gesamthochschule, D-4790 Paderborn, FRG, Department of Chemistry, Victoria University of Wellington, P.O. Box 600, Wellington, New Zealand, and Laboratoire de Chimie Inorganique, Institut de Chimie Moléculaire d'Orsay, Université de Paris-Sud, F-91405 Orsay, France. *Received June 20, 1991*

Abstract: Synthesis of asymmetric *hetero*dinuclear complexes $[LM^1(\mu\text{-}O)(\mu\text{-}CH_3CO_2)_2M^2L']^{2+}$, where L represents 1,4,7-triazacyclononane, L' is 1,4,7-trimethyl-1,4,7-triazacyclononane, and M^1 and M^2 are two different trivalent first-row transition metals, has been achieved by the hydrolytic reaction of an equimolar mixture of LM^1Cl_3 and $L'M^2Cl_3$ in aqueous sodium acetate solution. The asymmetric *homo*dinuclear species $[LM(\mu\text{-}O)(\mu\text{-}CH_3CO_2)_2ML']^{2+}$ (M = Mn^{III} (**1**), Fe^{III} (**2**)) have also been prepared. The following heterodinuclear species have been isolated as PF_6^- or ClO_4^- salts and characterized: $Fe^{III}Mn^{III}$ (**3**), $Fe^{III}Cr^{III}$ (**4**), $Cr^{III}Mn^{III}$ (**5**), and $Cr^{III}V^{III}$ (**7**). **4** is protonated in acidic solution affording the μ-hydroxo bridged complex $[L'Cr(\mu\text{-}OH)(\mu\text{-}CH_3CO_2)_2FeL](ClO_4)_3\cdot 2H_2O$ (**4H**). Oxidation of **3** and **5** in aqueous solution with $Na_2S_2O_8$ gave $[L'Fe^{III}(\mu\text{-}O)(\mu\text{-}CH_3CO_2)_2Mn^{IV}L](ClO_4)_3\cdot H_2O$ (**8**) and $[L'Cr^{III}(\mu\text{-}O)(\mu\text{-}CH_3CO_2)_2Mn^{IV}L](ClO_4)_3$ (**6**). The crystal structures of the ClO_4^- salts of **3**, **5**, and **6** and the PF_6^- salt of **4** have been determined by single crystal X-ray crystallography: **3**, monoclinic $C2/c$, $a = 23.929$ (6) Å, $b = 19.036$ (5) Å, $c = 16.701$ (3) Å, $\beta = 119.52$ (1)°, $Z = 8$; **4**, orthorhombic $Pbca$, $a = 18.951$ (4) Å, $b = 14.160$ (5) Å, $c = 24.619$ (5) Å, $Z = 8$; **5**, monoclinic $P2_1/c$, $a = 11.146$ (2) Å, $b = 20.975$ (4) Å, $c = 13.563$ (3) Å, $\beta = 99.71$ (2)°, $Z = 4$. **6**, monoclinic $P2_1/m$, $a = 11.332$ (3) Å, $b = 9.715$ (1) Å, $c = 16.180$ (4) Å, $\beta = 110.16$ (1)°, $Z = 2$. Bulk magnetic properties of all compounds have been studied in the temperature range 4.2-298 K. It has been found that the spins of the two paramagnetic metal ions are either intramolecularly antiferromagnetically (**2**, **3**, **4**, **4H**, **6**, **8**) or ferromagnetically coupled (**1**, **5**, **7**). An analysis of the interacting magnetic orbitals in complexes containing the μ-oxo-bis(μ-carboxylato)dimetal core is presented.

Introduction

Electronic and magnetic properties of dinuclear oxo-bridged iron proteins have in the past two decades received the attention of biochemists, inorganic chemists, and physicists.[2] This class of non-heme metalloproteins contains, as a common structural feature in their fully oxidized forms, two high-spin ferric ions which are bridged by one oxo ligand and, in addition, by one or two carboxylates. Structurally characterized examples are azidomethemerythrin,[3] hemerythrin, and, very recently, ribonucleotide reductase[4] all of which contain a bent Fe^{III}–O–Fe^{III} moiety. Other metalloproteins which are believed to contain this unit in its ferric form are the purple acid phosphatases[5] and uteroferrin. In all cases a strong antiferromagnetic coupling of the unpaired spins

‡Present address: CEMES LOE, UPR A 8011, BP 4347, 29, Rue Jeanne Marvig, F-31055 Toulouse, France.

(1) (a) Ruhr-Universität Bochum. (b) Universität Paderborn. (c) Victoria University of Wellington. (d) Université de Paris-Sud.

(2) (a) Lippard, S. J. *Angew. Chem., Int. Ed. Engl.* **1988**, *27*, 344. (b) Sanders-Loehr, J. In *Physical Bioinorganic Chemistry 5: Iron Carriers and Iron Proteins*; Loehr, T. M., Ed.; VCH Publishers: New York, Weinheim, Cambridge, 1989; p 373. (c) Kurtz, D. M., Jr. *Chem. Rev.* **1990**, *90*, 585. (e) Que, L., Jr.; True, A. E. *Progr. Inorg. Chem.* **1990**, *38*, 97.

(3) (a) Stenkamp, R. E.; Sieker, L. C.; Jensen, L. H. *J. Am. Chem. Soc.* **1984**, *106*, 618. (b) Sieker, L. C.; Stenkamp, R. E.; Jensen, L. H. In *The Biological Chemistry of Iron*; Dunford, H. B., Dolphin, D., Raymond, K. N., Sieker, L. C., Eds.; D. Reidel Publishing Company: Boston, MA, 1982; p 161. (c) Holmes, M. A.; Trong, I. L.; Turley, S.; Sieker, L. C.; Stenkamp, R. E. *J. Mol. Biol.* **1991**, *218*, 583.

0002-7863/92/1514-1681$03.00/0

Table I. Comparison of Structural Data and Magnetic Properties of Homodinuclear Complexes Containing the μ-Oxo-bis(μ-carboxylato)dimetal(III) Core

complex	M–O_{oxo}, Å	M···M, Å	M–O–M, deg	[(M–N_{trans}) – (M–N_{cis})], Å[a]	magnetism J,[b] cm^{-1}	ref
$[L'_2Ti_2(O)(PhCO_2)_2]^{2+}$	1.82 (2)	3.198 (4)	122.7 (8)	+0.10	diamagnetic	17
$[L'_2V_2(O)(CH_3CO_2)_2]^{2+}$	1.792 (4)	3.250 (2)	130.2 (2)	+0.07	>+400	18
$[L'_2Cr_2(O)(CH_3CO_2)_2]^{2+}$	1.850 (5)	3.219 (2)	121.0 (3)	+0.036	−56	48
$[L'_2Mn_2(O)(CH_3CO_2)_2]^{2+}$	1.810 (4)	3.096 (2)	119.9 (3)	−0.10	+18	13a,c
$[L_2Mn_2(O)(CH_3CO_2)_2]^{2+}$	1.788 (6)	3.096 (2)	119.9 (3)	−0.115	ferromagnetic	13b
$[(HBpz_3)_2Mn_2(O)(CH_3CO_2)_2]$	1.780 (2)	3.159 (1)	125.1 (1)	−0.117	−1.0	9
$[(bpy)_2(H_2O)_2Mn_2(O)(CH_3CO_2)_2]^{2+}$	1.783 (5)		122.9	−0.008	−6.8	14a
$[(bpy)_2Mn_2Cl_2(O)(CH_3CO_2)_2]$		3.153 (3)			−8.2	14b, 7b
$[(bpy)_2Mn_2(N_3)_2(O)(PhCO_2)_2]$	1.802	3.153 (4)	122.0 (5)	−0.050	+6.8	14b, 7b
$[L'_2Fe_2(O)(CH_3CO_2)_2]^{2+}$	1.800 (3)	3.120 (4)	119.7 (1)	+0.07	−238	16
$[(HBpz_3)_2Fe_2(O)(CH_3CO_2)_2]$	1.784 (2)	3.146 (1)	123.6 (1)	+0.038	−240	19
$[(bpy)_2Cl_2Fe_2(O)(CH_3CO_2)_2]$	1.785 (4)	3.151 (1)	123.9 (2)	+0.056	−264	20

[a] This column gives the difference between metal–nitrogen bonds in trans position to the M–O_{oxo} bond and the respective (averaged) M–N bond lengths in cis position to the M–O_{oxo} bond. [b] $\mathcal{H} = -JS_1 \cdot S_2$; abbreviations: L' = 1,4,7-trimethyl-1,4,7-triazacyclononane, L = 1,4,7-triazacyclononane, $HBpz_3$ = hydrotrispyrazolylborate(1−), bpy = 2,2'-bipyridine, Ph = phenyl.

of the iron(III) ions is thought to be mediated by an oxo bridge via a magnetic superexchange pathway.[6]

Interestingly, there appears to be a similar class of metalloproteins containing manganese as the essential transition metal.[7] Fridovich's pseudocatalase isolated from *Lactobacillus plantarum* contains a dinuclear active site (Mn^{III})[8] with bridging oxo ligands as judged by its electronic[9] and ESR spectra.[10] A catalase isolated from *Thermus thermophilus* has been shown by X-ray crystallography and ESR spectroscopy to contain two manganese ions at ≈3.6 Å distance.[11] Finally, a dinuclear active site has also been suggested for a manganese containing ribonucleotide reductase isolated from *Brevibacterium ammoniagenes*, although the evidence for this site is at present meager.[12]

Over the past years an impressive number of low molecular weight model complexes which contain a μ-oxo-bis(μ-carboxylato)dimetal(III) core (metal = Fe^{III},[2] Mn^{III}[7]) have been synthesized and structurally characterized and their electronic and magnetic properties have been studied in detail. One of the most intriguing facets of these studies is the discovery that magnetic exchange coupling in dinuclear oxo-bridged ferric (d^5) complexes is invariably strongly antiferromagnetic ($\mathcal{H} = -JS_1 \cdot S_2$, $S_1 = S_2 = {}^5/_2$; $J \approx -200\ cm^{-1}$) giving rise to an $S = 0$ ground state, whereas for the analogous manganese(III) compounds the situation is more complex. Consider for example the following three model complexes (a),[13] (b),[9] and (c)[14] where the two high-spin (hs) manganese(III) ions (d^4) are bridged by an oxo and two carboxylato ligands. The geometry and the dimensions of the bridging core structure are quite similar, only the capping

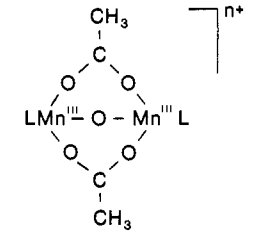

a: L = 1,4,7-trimethyl-1,4,7-triazacyclononane, n=2

b: L = hydro-tris(pyrazolyl)borate, n=0

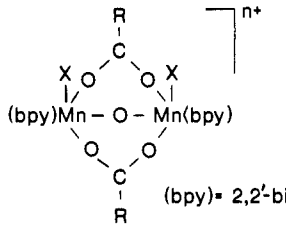

c: X = H_2O; R = CH_3, n=2

d: X = Cl^-; R = C_6H_5, n=0

e: X = N_3^-; R = C_6H_5, n=0

ligands and the overall charges differ. Despite the structural similarity the nature of the magnetic exchange interaction changes from weakly ferromagnetic in (a) to nearly uncoupled in (b) to weakly antiferromagnetic in (c). In complexes (d) and (e) the coupling also changes from weakly antiferromagnetic to weakly ferromagnetic although only the terminal chloride ligands are substituted by azide ions.[7b,14b]

In an early attempt to rationalize these observations it was stated[9] that "the d_{z^2} orbitals directed along the M–O_{oxo} bond vectors are occupied in the hs d^5-Fe^{III} compounds but unoccupied in the high-spin d^4 Mn^{III} analogues. This difference eliminates a major pathway for orbital coupling in the Mn^{III} compared with the Fe^{III} complexes and leads to a markedly diminished magnetic exchange interaction". This implies that the major superexchange path in bent Fe–O–Fe species is mediated between two d_{z^2} orbitals by a p-orbital of the oxo bridge.

In order to test this hypothesis we have recently prepared the symmetric heterodinuclear complex $[L'Mn^{III}(\mu\text{-}O)(\mu\text{-}CH_3CO_2)_2Fe^{III}L']^{2+}$[15] (L' represents the tridentate capping ligand 1,4,7-trimethyl-1,4,7-triazacyclononane) which contains a hs d^5

(4) (a) Sjöberg, B.-M.; Gräslund, A. *Adv. Inorg. Biochem.* **1983**, *5*, 87. (b) Lammers, M.; Follmann, H. *Struct. Bonding* **1983**, *54*, 27. (c) Nordlund, P.; Sjöberg, B.-M.; Eklund, H. *Nature* **1990**, *345*, 593.

(5) (a) Antanaitis, B. C.; Aisen, P. *Adv. Inorg. Biochem.* **1983**, *5*, 111. (b) Que, L., Jr.; Scarrow, R. C. In *Metal Clusters in Proteins*; Que, L., Jr., Ed.; ACS Symposium Series 372; Washington, DC, 1988; p 152.

(6) Murray, K. S. *Coord. Chem. Rev.* **1974**, *12*, 1.

(7) (a) Wieghardt, K. *Angew. Chem., Int. Ed. Engl.* **1989**, *28*, 1153. (b) Christou, G. *Acc. Chem. Res.* **1989**, *22*, 328.

(8) (a) Kono, Y.; Fridovich, I. *J. Biol. Chem.* **1983**, *258*, 6015, 13646. (b) Beyer, W. F., Jr.; Fridovich, I. *Biochemistry* **1985**, *24*, 6460.

(9) Sheats, J. E.; Czernuszewics, R. S.; Dismukes, G. C.; Rheingold, A. L.; Petrouleas, V.; Stubbe, J.; Armstrong, W. H.; Beer, R. H.; Lippard, S. J. *J. Am. Chem. Soc.* **1987**, *109*, 1435.

(10) Fronko, R. M.; Penner-Hahn, J. E.; Bender, C. J. *J. Am. Chem. Soc.* **1988**, *110*, 7554.

(11) (a) Barynin, V. V.; Grebenko, A. I. *Dokl. Akad. Nauk SSR* **1986**, *288*, 1100. (b) Barynin, V. V.; Vagin, A. A.; Melik-Adamyan, V. R.; Grebenko, A. I.; Khangulov, S. V.; Popov, A. N.; Andrianova, M. E.; Vainshtein, B. K. *Dokl. Akad. Nauk SSR* **1986**, *288*, 877. (c) Vainshtein, B. K.; Melik-Adamyan, V. R.; Barynin, V. V. *Kristollografia* **1981**, *26*, 10003. (d) Khangulov, S. V.; Barynin, V. V.; Melik-Adamyan, V. R.; Grebenko, A. I.; Voevodskaya, N. V.; Blumenfeld, L. A.; Dobryakov, S. N. *Bioorg. Khim.* **1986**, *12*, 741. (e) Khangulov, S. V.; Voevodskaya, N. V.; Barynin, V. V.; Grebenko, A. I.; Melik-Adamyan, V. R. *Biofizika* **1987**, *32*, 960.

(12) (a) Willing, A.; Follmann, H.; Auling, G. *Eur. J. Biochem.* **1988**, *170*, 603. (b) Plonzig, J.; Auling, G. *Arch. Microbiol.* **1987**, *146*, 396.

(13) (a) Wieghardt, K.; Bossek, U.; Ventur, D.; Weiss, J. *J. Chem. Soc., Chem. Commun.* **1985**, 347. (b) Bossek, U.; Wieghardt, K.; Nuber, B.; Weiss, J. *Inorg. Chim. Acta* **1989**, *165*, 123. (c) Wieghardt, K.; Bossek, U.; Nuber, B.; Weiss, J.; Bonvoisin, J.; Corbella, M.; Vitols, S. E.; Girerd, J. J. *J. Am. Chem. Soc.* **1988**, *110*, 7398.

(14) (a) Ménage, S.; Girerd, J. J.; Gleizes, A. *J. Chem. Soc., Chem. Commun.* **1988**, 431. (b) Vincent, J. B.; Folting, K.; Huffman, J. C.; Christou, G. *Biochem. Soc. Trans.* **1988**, *16*, 822.

(15) Bossek, U.; Weyhermüller, T.; Wieghardt, K.; Bonvoisin, J.; Girerd, J. J. *J. Chem. Soc., Chem. Commun.* **1989**, 633.

Fe^{III} and a hs d^4 Mn^{III} ion in exactly the same ligand environment as the homodinuclear Fe_2^{III}[16] and Mn_2^{III}[13] species. In contrast to the anticipated uncoupled behavior (the d_{z^2} orbital of the Mn^{III} site is empty) strong antiferromagnetic coupling is observed ($S = {}^1/_2$ ground state; $J = -145$ cm^{-1}; $\mathcal{H} = -JS_1 \cdot S_2$, $S_1 = {}^5/_2$; $S_2 = {}^4/_2$).

Furthermore, extension of the homodinuclear series $[L'_2M_2(\mu\text{-}O)(\mu\text{-}CH_3CO_2)_2]^{2+}$ to complexes containing the first-row transition-metals Ti^{III}, d^1,[17] V^{III}, d^2,[18] and Cr^{III}, d^3[48] resulted in the discovery that the Ti^{III} complex is diamagnetic ($S = 0$), the V^{III} complex has four fully aligned spins ($S = 2$) over the temperature range 4.2–298 K, and the Cr^{III} complex is weakly antiferromagnetically coupled (Table I). These results suggest a more complex picture of the magnetic exchange pathways.

In order to obtain an understanding of the relevant magnetic exchange pathways within this biologically important μ-oxo-bis(μ-carboxylato)dimetal structural unit we have synthesized *asymmetric* heterodinuclear complexes of this type which contain the capping ligand 1,4,7-triazacyclononane (L) coordinated to one metal and its N-methylated derivative L′ bound to the other metal ion. By incorporating different d^n and d^m electron configurations at the two metal sites it was hoped to identify the relevant magnetic exchange pathways.

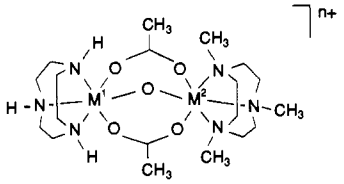

Experimental Section

The ligands 1,4,7-triazacyclononane (L) and its methylated derivative 1,4,7-trimethyl-1,4,7-triazacyclononane (L′) were prepared according to published procedures. The monomeric precursor complexes $LMCl_3$ (M = V,[18] Mn,[13] Fe[16b]), $L'MCl_3$ (M = V,[18] Cr,[22] Mn,[13] Fe[16b]), and the homodinuclear species $[L_2M_2O(CH_3CO_2)_2](ClO_4)_2$ (M = Fe,[16] Mn[13]) were prepared as described previously.

Elemental analyses of complexes were performed as follows: The metal content of heterodinuclear species was determined spectrophotometrically according to Hartkamp's[24] procedures: Fe^{III}, Mn^{III} as bis(pyridine-2,6-dicarboxylato)metal(III) complexes, and V as $[VO(dipic)(O_2)]^-$. Determination of the chromium content was also carried out spectrophotometrically as CrO_4^{2-}. In some cases perchlorate was determined gravimetrically as $[AsPh_4]ClO_4$.

Preparation of Complexes. **$[LMnO(CH_3CO_2)_2MnL'](ClO_4)_2$ (1).** An equimolar mixture of $LMnCl_3$ (0.45 g, 1.5 mmol) and $L'MnCl_3$ (0.5 g, 1.5 mmol) was dissolved in methanol (30 mL) at room temperature with stirring. Upon addition of sodium acetate (1 g) a clear red-purple solution was obtained to which $NaClO_4$ (2 g) was added. Red-purple crystals precipitated which were collected by filtration and recrystallized from methanol: 0.87 g (80% yield). The complex may also be obtained as bis(hexafluorophosphate)hydrate salt by using $NaPF_6$ instead of $NaClO_4$. Anal. Calcd for $[C_{19}H_{42}N_6O_5Mn_2](ClO_4)_2$: C, 30.70; H, 5.70; N, 11.30; Mn, 14.78. Found: C, 30.5; H, 5.9; N, 11.2; Mn, 14.6.

$[LFeO(CH_3CO_2)_2FeL'](PF_6)_2 \cdot H_2O$ (2). This complex was prepared as described above for (1) by using $LFeCl_3$ and $L'FeCl_3$ as starting materials and $NaPF_6$ to precipitate orange-brown crystals: 0.40 g (31% yield). Adding $NaClO_4$ instead of $NaPF_6$ yields the bisperchlorate salt. Anal. Calcd for $[C_{19}H_{42}N_6O_5Fe_2](PF_6)_2 \cdot H_2O$: C, 26.72; H, 5.19; N, 9.84; Fe, 13.08. Found: C, 26.6; H, 5.0; N, 9.9; Fe, 13.2.

$[LMnO(CH_3CO_2)_2FeL'](PF_6)_2 \cdot H_2O$ (3). To a solution of sodium acetate (4.0 g) in water (80 mL) were added $L'FeCl_3$ (0.75 g, 2.2 mmol) and $LMnCl_3$ (0.65 g, 2.2 mmol) with stirring at 25 °C. After ≈3 h a clear deep red-brown solution was obtained, and KPF_6 (5 g) was added which initiated the precipitation of brown microcrystals which were collected by filtration and recrystallized from water: 1.40 g (75% yield). The bisperchlorate salt was obtained by adding $NaClO_4$ instead of KPF_6. Anal. Calcd for $[C_{19}H_{42}N_6O_5FeMn](PF_6)_2 \cdot H_2O$: C, 26.74; H, 5.20; N, 9.85; Mn, 6.44; Fe, 6.54. Found: C, 26.6; H, 5.0; N, 9.5; Mn, 6.2; Fe, 6.5.

$[L'MnO(CH_3CO_2)_2FeL](PF_6)_2 \cdot H_2O$ (3a). This isomer of 3 was prepared as described by using $L'MnCl_3$ and $LFeCl_3$ as starting materials (yield: 80%). Anal. Calcd for $[C_{19}H_{42}N_6O_5FeMn](PF_6)_2 \cdot H_2O$: C, 26.74; H, 5.20; N, 9.85; Mn, 6.44; Fe, 6.54. Found: C, 26.7; H, 4.9; N, 9.7; Mn, 6.2; Fe, 6.4.

$[L'CrO(CH_3CO_2)_2FeL](ClO_4)_2 \cdot H_2O$ (4). A suspension of $L'CrBr_3$ (0.16 g, 0.34 mmol), $LFeCl_3$ (0.10 g, 0.34 mmol), and sodium acetate (1.0 g) in methanol (50 mL) was heated to reflux for 1.5 h. To the clear blue solution $NaClO_4$ (1 g) was added at 20 °C. Within 2–3 days at −18 °C blue-black crystals precipitated which were collected by filtration, washed with ethanol and ether, and dried: 0.15 g (58% yield). The bishexafluorophosphate salt was obtained when $NaPF_6$ (0.8 g) was added to the above solution instead of $NaClO_4$: 0.2 g (70% yield). Anal. Calcd for $[C_{19}H_{42}N_6O_5CrFe](ClO_4)_2 \cdot H_2O$: C, 30.1; H, 5.8; N, 11.1; ClO_4, 26.2; Fe, 7.4. Found: C, 30.3; H, 5.7; N, 10.9; ClO_4, 26.4; Fe, 7.6.

$[L'Cr(OH)(CH_3CO_2)_2FeL](ClO_4)_3 \cdot 2H_2O$ (4H). To a solution of 4 (0.24 g, 0.32 mmol) in methanol (20 mL) was added concentrated $HClO_4$ (1 mL). The color changed immediately from blue to orange, and microcrystals precipitated which were collected by filtration, washed with ether, and dried: 0.27 g (95% yield). Anal. Calcd for $[C_{19}H_{43}N_6O_5CrFe](ClO_4)_3 \cdot 2H_2O$: C, 26.0; H, 5.4; N, 9.6; ClO_4, 34.0; Fe, 6.4; Cr, 5.9. Found: C, 25.8; H, 5.2; N, 9.7; ClO_4, 34.8; Fe, 6.6; Cr, 6.0.

$[L'CrO(CH_3CO_2)_2MnL](ClO_4)_2$ (5). A mixture of $L'CrBr_3$ (0.13 g, 0.28 mmol), $[L_2Mn_2O(CH_3CO_2)_2](ClO_4)_2$ (0.10 g, 0.14 mmol) and sodium acetate (1.0 g) in methanol (50 mL) was heated under reflux for 1.5 h until a clear deep red solution was obtained. Upon addition of $NaClO_4$ (1.2 g) and cooling to 5 °C black-red crystals precipitated which were filtered off and washed with ethanol and ether and dried: 0.11 g (53% yield). Anal. Calcd for $[C_{19}H_{42}N_6O_5CrMn](ClO_4)_2$: C, 30.8; H, 5.7; N, 11.4; Mn, 7.4; Cr, 7.0. Found: C, 31.1; H, 5.5; N, 11.1; Mn, 7.7; Cr, 7.1.

The bishexafluorophosphate salt was prepared by a slightly different procedure. A mixture of $L'CrBr_3$ (0.16 g, 0.34 mmol), sodium acetate (1.0 g), and $LMnCl_3$ (0.10 g, 0.34 mmol) in methanol (50 mL) was heated under reflux for 1.5 h. To the resulting clear, deep red solution was added $NaPF_6$ (0.8 g) dissolved in methanol (10 mL). Upon cooling to 0 °C red-black crystals precipitated: 0.13 g (46% yield). Anal. Calcd for $[C_{19}H_{42}N_6O_5CrMn](PF_6)_2$: C, 27.5; H, 5.1; N, 10.1. Found: C, 27.7; H, 4.9; N, 9.8.

$[L'CrO(CH_3CO_2)_2MnL](ClO_4)_3$ (6). To a solution of 5 (0.20 g, 0.27 mmol) in water (20 mL) was added $Na_2S_2O_8$ (0.20 g) dissolved in H_2O (5 mL). The color of the solution changed from deep-red to brown. Upon addition of $NaClO_4$ (1.0 g) brown crystals precipitated out which were filtered off, washed with ether, and air dried: 0.16 g (71% yield). Using $NaPF_6$ instead of $NaClO_4$ yields the trishexafluorophosphate salt. Anal. Calcd for $[C_{19}H_{42}N_6O_5CrMn](ClO_4)_3$: C, 27.2; H, 5.0; N, 10.0; ClO_4, 35.5; Mn, 6.5; Cr, 6.2. Found: C, 26.8; H, 5.1; N, 9.9; ClO_4, 34.5; Mn, 6.6; Cr, 6.1.

$[L'CrO(CH_3CO_2)_2VL](ClO_4)_2$ (7). A mixture of sodium acetate (1.2 g), $L'CrBr_3$ (0.16 g, 0.34 mmol), and $LVCl_3$ (0.10 g, 0.34 mmol) in methanol (50 mL) was heated under reflux and an argon atmosphere for 1.5 h. Upon addition of $NaClO_4$ (1.2 g) to the green, clear solution and cooling to −18 °C for 2–3 days black-green crystals precipitated, which were collected by filtration, washed with ethanol and ether, and dried: 0.09 g (36% yield). Anal. Calcd for $[C_{19}H_{42}N_6O_5CrV](ClO_4)_2$: C, 31.0;

(16) (a) Chaudhuri, P.; Wieghardt, K.; Nuber, B.; Weiss, J. *Angew. Chem., Int. Ed. Engl.* **1985**, *24*, 778. (b) Hartmann, J. A.; Rardin, R. L.; Chaudhuri, P.; Pohl, K.; Wieghardt, K.; Nuber, B.; Weiss, J.; Papaefthymiou, G. C.; Frankel, R. B.; Lippard, S. J. *J. Am. Chem. Soc.* **1987**, *109*, 7387.

(17) Bodner, A.; Drüeke, S.; Wieghardt, K.; Nuber, B.; Weiss, J. *Angew. Chem., Int. Ed. Engl.* **1990**, *29*, 68.

(18) (a) Knopp, P.; Wieghardt, K.; Nuber, B.; Weiss, J.; Sheldrick, W. S. *Inorg. Chem.* **1990**, *29*, 363. (b) Köppen, M.; Fresen, G.; Wieghardt, K.; Llusar, R. M.; Nuber, B.; Weiss, J. *Inorg. Chem.* **1988**, *27*, 721. (c) Wieghardt, K.; Köppen, M.; Nuber, B.; Weiss, J. *J. Chem. Soc., Chem. Commun.* **1986**, 1530.

(19) (a) Armstrong, W. H.; Lippard, S. J. *J. Am. Chem. Soc.* **1983**, *105*, 4837. (b) Armstrong, W. H.; Spool, A.; Papaefthymiou, G. C.; Frankel, R. B.; Lippard, S. J. *J. Am. Chem. Soc.* **1984**, *106*, 3653.

(20) Vincent, J. B.; Huffman, J. C.; Christou, G.; Li, Q.; Nanny, M. A.; Hendrickson, D. N.; Fong, R. H.; Fish, R. H. *J. Am. Chem. Soc.* **1988**, *110*, 6898.

(21) *International Tables for X-ray Crystallography*; Kynoch Press: Birmingham, England, 1975; Vol. IV: (a) Table 2.2, pp 99–101. (b) Table 2.3.1, pp 149–150.

(22) Chaudhuri, P.; Winter, M.; Küppers, H.-J.; Wieghardt, K.; Nuber, B.; Weiss, J. *Inorg. Chem.* **1987**, *26*, 3302.

(23) The cyclic voltammogram of 3 in CH_3CN (0.1 M $[TBA]PF_6$ supporting electrolyte, internal standard ferrocene) at a Pt electrode in the potential range +1.8 to −1.2 V vs Ag/AgCl (saturated LiCl in EtOH) shows a reversible one-electron wave at $E_{1/2}$ 0.40 V vs Fc^+/Fc and a quasireversible process at E −0.71 V vs Fc^+/Fc. The cyclic voltammogram of **3a** shows under the same conditions a reversible one-electron transfer wave at $E_{1/2}$ 0.47 V vs Fc^+/Fc and an irreversible process at E − 0.69 V vs Fc^+/Fc.

(24) Hartkamp, H. (a) Mn: *Z. Analyt. Chem.* **1964**, *199*, 183. (b) Fe: *Z. Analyt. Chem.* **1962**, *190*, 66. (c) V: *Z. Analyt. Chem.* **1959/1960**, *171*, 262.

H, 5.8; N, 11.4; V, 6.9; Cr, 7.1. Found: C, 30.9; H, 6.0; N, 11.2; V, 6.9; Cr, 7.0.

$[L'FeO(CH_3CO_2)_2MnL](ClO_4)_3\cdot H_2O$ (8). To a solution of the perchlorate salt of **3** (0.70 g, 0.9 mmol) in methanol (30 mL) and water (10 mL) was added concentrated $HClO_4$ (3 mL) which initiated the precipitation of green microcrystals which were collected by filtration: 0.18 g (50% yield). Anal. Calcd for $[C_{19}H_{42}N_6O_5FeMn](ClO_4)_3\cdot H_2O$: C, 26.5; H, 5.2; N, 9.8; Mn, 6.4; Fe, 6.5. Found: C, 26.4; H, 5.0; N, 9.6; Mn, 6.3; Fe, 6.4.

$[LFeO(CH_3CO_2)_2MnL'](ClO_4)_3\cdot H_2O$ (8a). This isomer of **8** has been prepared as described above using the perchlorate salt of **3a** as starting material. Anal. Calcd for $[C_{19}H_{42}N_6O_5FeMn](ClO_4)_3\cdot H_2O$: C, 26.5; H, 5.2; N, 9.8; Mn, 6.4; Fe, 6.5. Found: C, 26.4; H, 5.0; N, 9.5; Mn, 6.4; Fe, 6.5.

The trishexafluorophosphate salts of **8** and **8a** were prepared by adding 0.5 g of $Na_2S_2O_8$ to an aqueous solution (30 mL) of **3** and **3a** (0.5 g), respectively. The color of the solutions slowly changed from brown to dark green. Upon addition of KPF_6 (1 g) green-brown microcrystals precipitated which were filtered off, washed with ethanol and ether, and air dried (yield: ≈ 50%). Anal. Calcd for $[C_{19}H_{42}N_6O_5FeMn](PF_6)_3$: C, 23.3; H, 4.3; N, 8.6. Found: C, 23.7; H, 4.5; N, 8.9 **[8]**$(PF_6)_3$. C, 23.5; H, 4.5; N, 8.5 **[8a]**$(PF_6)_3$.

X-ray Crystallography. Intensities and lattice parameters of a green, column-shaped crystal of **3**, a blue-green, irregularly shaped crystal of **4**, a red, tabular-shaped crystal of **5**, and a brown, column-shaped crystal of **6** were measured at ambient temperature on a Nicolet R 3m/V diffractometer by using graphite monochromated Mo K_α radiation. Crystal parameters and details of the data and reduction are given in Table II. Empirical absorption corrections (ψ-scans) were carried out in each case. All structures were solved by direct and Fourier methods and refined with anisotropic thermal parameters for all non-hydrogen atoms—except the carbon atoms of the macrocyclic ligands which were refined with isotropic thermal parameters. Neutral atom scattering factors were calculated by the standard procedures.[21a] Anomalous dispersion corrections were applied to all non-hydrogen atoms.[21b] H-atom positions of methylene and methyl groups were calculated from geometrical considerations (C–H 0.96 Å, sp^3-hybridized C). One of the ClO_4^- ions in the crystal of **3** was found to be disordered. This disorder was successfully modeled by introducing two different sites with occupancy factor 0.5 for the Cl and O atoms (Cl2 and Cl3), respectively (see supplementary material).

Magnetic Susceptibility Measurements. Measurements of the molar susceptibility were carried out on solid samples by using the Faraday method between 4.2 and 298 K. The magnetic susceptibilities were corrected for diamagnetism by using Pascal's constants.

Results

Synthesis. The synthesis of a series of dinuclear complexes with two different first-row transition metals, i.e., a chromium(III) and a divalent metal ion (Zn^{II}, Cu^{II}, Ni^{II}, Co^{II}, Fe^{II}, and Mn^{II}), the μ-hydroxo-bis(μ-acetato)dimetal core, and a capping 1,4,7-trimethyl-1,4,7-triazacyclononane ligand on each metal center have been reported.[22] Hereafter these are called *symmetric* heterodinuclear complexes where the term symmetric pertains to the fact that the two tridentate capping ligands at both metal ions are identical, in contrast to *asymmetric* species which contain two different capping ligands. Since the metal-to-nitrogen (and oxygen) bond distances at the trivalent and divalent ion are sufficiently different, it is possible to distinguish by X-ray crystallography between the two metal sites in these symmetric species. No crystallographically imposed symmetry is observed in the structure determinations of the respective perchlorate salts.

This situation changes when both first-row transition metals in the symmetric dinuclear complexes of the type $[L'_2M^1M^2(\mu\text{-}O)(\mu\text{-}CH_3CO_2)_2]^{2+}$ are trivalent. Thus $[L'_2Mn^{III}Fe^{III}(\mu\text{-}O)(\mu\text{-}CH_3CO_2)_2](ClO_4)_2\cdot H_2O$[15] was found to crystallize in the same space group with very similar unit cell dimensions as its homodinuclear counterparts $[L'_2Mn_2^{III}(\mu\text{-}O)(\mu\text{-}CH_3CO_2)_2](ClO_4)_2\cdot H_2O$[13a] and $[L'_2Fe_2^{III}(\mu\text{-}O)(\mu\text{-}CH_3CO_2)_2](ClO_4)_2\cdot H_2O$.[16] In this space group the dications possess crystallographically required site symmetry *mm*, and it is not possible to distinguish between the two metal ions in a symmetric heterodinuclear complex of this kind by X-ray crystallography. This is due to the fact that the M^{III}–N and M^{III}–O bond lengths at both metal ions are, in general, similar.

A further disadvantage for the preparation of pure samples of heterodinuclear species via spontaneous self-assembly starting with mononuclear precursors containing the same capping ligand is the difficulty in assessing the purity of the crystalline material obtained because solubility products of symmetric homo- and heterodinuclear species may be quite similar and cocrystallization of both species may occur.

In order to avoid these complications we decided to synthesize *asymmetric* heterodinuclear complexes which should be readily purified by recrystallization. We found that hydrolysis of an equimolar mixture of mononuclear precursors LM^1Cl_3 and $L'M^2Cl_3$ (L represents the facially coordinated amine 1,4,7-triazacyclononane and L' its N-methylated derivative 1,4,7-trimethyl-1,4,7-triazacyclononane) in methanol solution containing sodium acetate affords in good yields asymmetric dinuclear complexes containing the μ-oxo-bis(μ-acetato)dimetal(III) core, eq 1.

$$LM^1Cl_3 + L'M^2Cl_3 \xrightarrow[H_2O]{ac^-} [LM^1(\mu\text{-}O)(\mu\text{-}CH_3CO_2)_2M^2L']^{2+} \quad (1)$$

If M^1 and M^2 represent the same trivalent metal ion, e.g., Mn^{III} or Fe^{III}, we have been able to isolate the asymmetric *homo*dinuclear complexes $[L'Mn^{III}(\mu\text{-}O)(\mu\text{-}CH_3CO_2)_2Mn^{III}L](ClO_4)_2$ (**1**) or $[L'Fe(\mu\text{-}O)(\mu\text{-}CH_3CO_2)_2FeL](PF_6)_2\cdot H_2O$ (**2**) as crystalline materials upon addition of $NaClO_4$ or $NaPF_6$ to the reaction mixtures. It is also possible to generate the asymmetric species **1** and **2** by heating 1:1 mixtures of the symmetric dinuclear complexes $[L_2M_2O(CH_3CO_2)_2](ClO_4)_2$ and $[L'_2M_2O(CH_3CO_2)_2](ClO_4)_2$ in methanol.

If M^1 and M^2 in eq 1 represent two different metal ions, there are in principle two geometric isomers possible depending on which metal is coordinated to which of the two tridentate amines. Thus if M^1 represents Mn^{III} and M^2 = Fe^{III}, the isomers $[LMnO(CH_3CO_2)_2FeL']^{2+}$ and $[L'MnO(CH_3CO_2)_2FeL]^{2+}$ should be and are available. Hydrolysis of a mixture of $LMnCl_3$ and $L'FeCl_3$ in water containing sodium acetate yields the former, whereas hydrolysis of $L'MnCl_3$ and $LFeCl_3$ affords the latter species; both isomers have been isolated as hexafluorophosphate salts (**3** and **3a**). The perchlorate salt of **3** has been characterized by X-ray crystallography. When reaction 1 was carried out at elevated temperatures and prolonged reaction times, ligand scrambling was observed, and both isomers **3** and **3a** formed in an approximately 1:1 ratio as was judged from their cyclic voltammograms.[23] As we will show subsequently the magnetic and electronic properties of these isomers do not differ significantly (although the redox potentials do). We have not prepared and characterized both isomers in all of the following cases, although in principle this is feasible.

The reaction of sodium acetate, $L'CrBr_3$ and $LFeCl_3$ in refluxing methanol affords upon addition of $NaClO_4$ blue crystals of $[L'Cr(\mu\text{-}O)(\mu\text{-}CH_3CO_2)_2FeL](ClO_4)_2\cdot H_2O$ (**4**) in 58% yield. Acidification of a methanolic solution of **4** with concentrated perchloric acid leads to the precipitation of orange crystals of $[L'Cr(\mu\text{-}OH)(\mu\text{-}CH_3CO_2)_2FeL](ClO_4)_3\cdot 2H_2O$ (**4H**) which is the protonated form of **4**, eq 2.

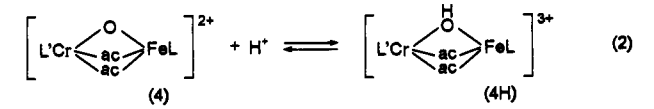

(4) (4H) (2)

Employing the same reaction conditions as described above for the synthesis of **4**, but using a mixture of $L'CrBr_3$ and $[L_2Mn_2(\mu\text{-}O)(\mu\text{-}CH_3CO_2)_2](ClO_4)_2$ in a ratio 2:1, affords black-red crystals of $[L'Cr^{III}(\mu\text{-}O)(\mu\text{-}CH_3CO_2)_2Mn^{III}L](ClO_4)_2$ (**5**). This experiment indicates that the symmetric homodinuclear manganese(III) complex dissociates at elevated temperatures in solution to produce a monomer which then forms the asymmetric heterodinuclear species with $L'CrBr_3$ in ≈50% yield. **5** is readily oxidized in aqueous solution by peroxodisulfate to the asymmetric $Cr^{III}Mn^{IV}$ dinuclear species **6** which was isolated as a brown crystalline perchlorate salt, eq 3.

Hydrolysis of a 1:1:40 mixture of $L'CrBr_3$, $LVCl_3$, and sodium acetate in methanol under anaerobic conditions yields black-green crystals of $[L'Cr^{III}(\mu\text{-}O)(\mu\text{-}CH_3CO_2)_2V^{III}L](ClO_4)_2$ (**7**).

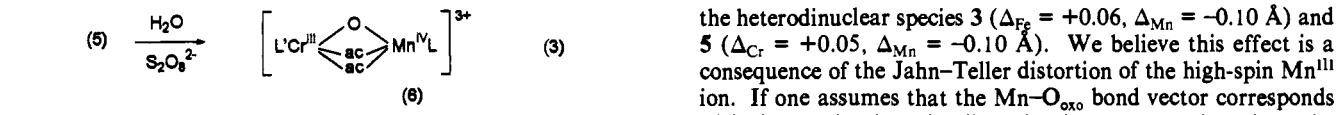

(6)

Previously we had observed[13c] that the symmetric homodinuclear complex $[L'_2Mn_2^{III}(\mu\text{-}O)(\mu\text{-}CH_3CO_2)_2]^{2+}$ disproportionates in acidic aqueous solution, and the mixed-valent $Mn^{III}Mn^{IV}$ species $[L'_2Mn_2(\mu\text{-}O)(\mu\text{-}CH_3CO_2)_2](ClO_4)_3$ had been isolated from such solutions in ≈50% yield.

From an electrochemical investigation a mechanism for this disproportionation reaction was proposed where the protonated species is the stronger oxidant, and, therefore, the protonated form oxidizes the oxo-bridged form. $Mn^{II}Mn^{III}$ and $Mn^{III}Mn^{IV}$ mixed-valent species are generated in a ratio 1:1. The $Mn^{II}Mn^{III}$ species dissociates in acidic aqueous solution, eqs 4 and 5.

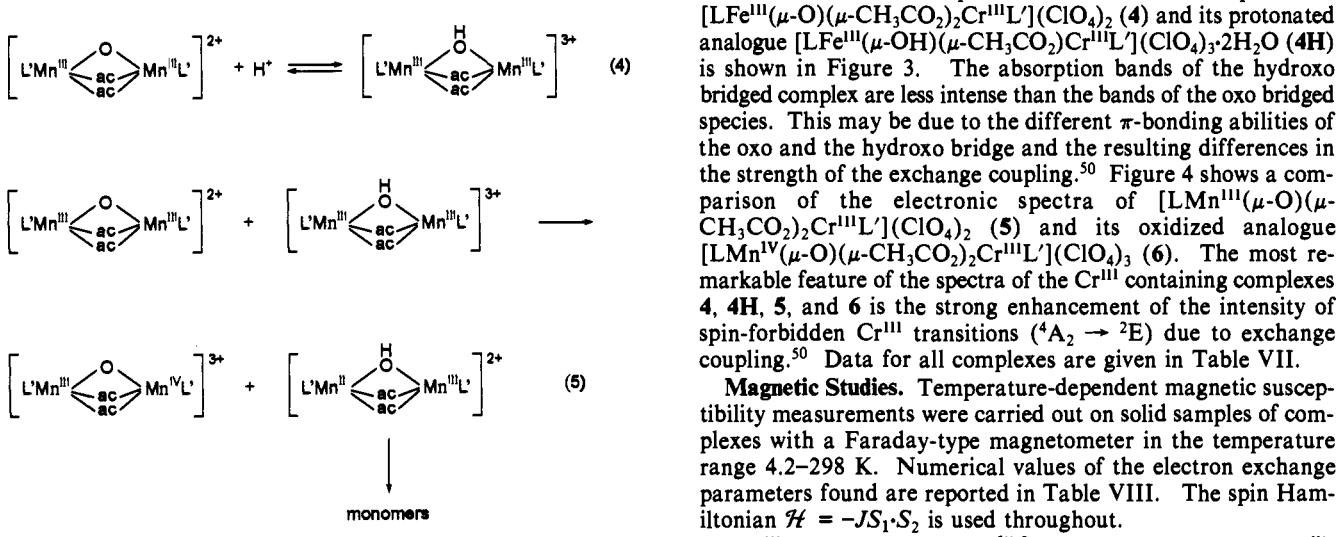

In line with this observation is the discovery that both asymmetric heterodinuclear $Fe^{III}Mn^{III}$ isomers **3** and **3a** also disproportionate in acidic aqueous solution producing the $Mn^{IV}Fe^{III}$ isomers **8** and **8a** in maximally 50% yield. **8** and **8a** were also obtained from aqueous solutions of **3** and **3a** by using $S_2O_8^{2-}$ as oxidant.

Crystal Structures. Four asymmetric complexes have been investigated by single-crystal X-ray diffraction methods: $Fe^{III}Mn^{III}$ (**3**), $Cr^{III}Fe^{III}$ (**4**), $Cr^{III}Mn^{III}$ (**5**), and $Cr^{III}Mn^{IV}$ (**6**). The cations in all three complexes possess the same overall structure; two different metal ions are connected by a μ_2-oxo group and two bidentate μ-acetato bridges. The remaining three coordination sites of the metals are occupied by a facially bound 1,4,7-triazacyclononane ligand L and by a 1,4,7-trimethyl-1,4,7-triazacyclononane ligand L'. Each metal ion is in a distorted octahedral environment (N_3O_3 donor set). Figure 1 shows the structures of the cations and their respective atom labeling scheme. Tables III–VI summarize important bond lengths and angles of the $N_3M^1(\mu\text{-}O)(\mu\text{-}CH_3CO_2)_2M^2N_3$ core in **3**, **4**, **5**, and **6**.

In the following we discuss some salient features of the structure of these asymmetric heterodinuclear complexes and of their symmetric homodinuclear counterparts: (i) The nonbonding distance between the metal ions M^1 and M^2 in homo- and heterodinuclear species varies between 3.25 and 3.11 Å. (ii) The $M\text{–}O_{oxo}$ bond distance varies between 1.85 and 1.78 Å which indicates considerable metal–oxygen double bond character; the $M^1\text{–}O\text{–}M^2$ bond angles are found to be in the range 110–130°. (iii) The short $M\text{–}O_{oxo}$ bond exerts a pronounced structural influence on the M–N bond in trans position with respect to the $M\text{–}O_{oxo}$. Thus in all cases, except those involving Mn^{III}, the $M\text{–}N_{trans}$ bond is longer than the average of the two $M\text{–}N_{cis}$ distances. The difference $\Delta[(M\text{–}N_{trans}) - (M\text{–}N_{cis})]$ is in the range +0.04 to +0.12 Å (Tables I, III–VI). In the Mn^{III} complexes the reverse behavior is observed; here the $Mn\text{–}N_{trans}$ bond is *shorter* than the $Mn\text{–}N_{cis}$ bonds (Δ = −0.01 to −0.12 Å). This holds for all homodinuclear complexes of this type reported to date and for the heterodinuclear species **3** (Δ_{Fe} = +0.06, Δ_{Mn} = −0.10 Å) and **5** (Δ_{Cr} = +0.05, Δ_{Mn} = −0.10 Å). We believe this effect is a consequence of the Jahn–Teller distortion of the high-spin Mn^{III} ion. If one assumes that the $Mn\text{–}O_{oxo}$ bond vector corresponds with the *z*-axis, then the distortion is a compression along the *z*-axis.[13b] In **6** which contains a Mn^{IV} (d^3) ion the $M\text{–}N_{trans}$ bond is again longer at both metal ions (Δ_{Cr} = +0.02, Δ_{Mn} = +0.04 Å). Thus it is possible to unambiguously assign the oxidation states of the metal ions in manganese containing species by X-ray crystallography.

Electronic Spectra. Figure 2 shows the electronic spectra of the asymmetric complexes $[LMn^{III}(\mu\text{-}O)(\mu\text{-}CH_3CO_2)_2Mn^{III}L'](PF_6)_2$ (**1**) and $[LFe^{III}(\mu\text{-}O)(\mu\text{-}CH_3CO_2)_2Fe^{III}L'](PF_6)_2\cdot H_2O$ (**2**). The corresponding symmetrical compounds exhibit very similar spectra which were discussed elsewhere.[13a,c,49] A comparison of the electronic spectra of $[LFe^{III}(\mu\text{-}O)(\mu\text{-}CH_3CO_2)_2Cr^{III}L'](ClO_4)_2$ (**4**) and its protonated analogue $[LFe^{III}(\mu\text{-}OH)(\mu\text{-}CH_3CO_2)Cr^{III}L'](ClO_4)_3\cdot 2H_2O$ (**4H**) is shown in Figure 3. The absorption bands of the hydroxo bridged complex are less intense than the bands of the oxo bridged species. This may be due to the different π-bonding abilities of the oxo and the hydroxo bridge and the resulting differences in the strength of the exchange coupling.[50] Figure 4 shows a comparison of the electronic spectra of $[LMn^{III}(\mu\text{-}O)(\mu\text{-}CH_3CO_2)_2Cr^{III}L'](ClO_4)_2$ (**5**) and its oxidized analogue $[LMn^{IV}(\mu\text{-}O)(\mu\text{-}CH_3CO_2)_2Cr^{III}L'](ClO_4)_3$ (**6**). The most remarkable feature of the spectra of the Cr^{III} containing complexes **4**, **4H**, **5**, and **6** is the strong enhancement of the intensity of spin-forbidden Cr^{III} transitions ($^4A_2 \rightarrow {}^2E$) due to exchange coupling.[50] Data for all complexes are given in Table VII.

Magnetic Studies. Temperature-dependent magnetic susceptibility measurements were carried out on solid samples of complexes with a Faraday-type magnetometer in the temperature range 4.2–298 K. Numerical values of the electron exchange parameters found are reported in Table VIII. The spin Hamiltonian $\mathcal{H} = -JS_1\cdot S_2$ is used throughout.

$[Mn^{III}(\mu\text{-}O)(\mu\text{-}CH_3CO_2)_2Mn^{III}]^{2+}$. The $\chi_M T$ value for the Mn^{III}_2 complex **1** increases from 6.41 $cm^3\ mol^{-1}\ K$ at 293.5 K to 8.43 $cm^3\ mol^{-1}\ K$ at 50.6 K. This is characteristic of a ferromagnetic coupling between the two high-spin Mn^{III} ions. A similar result was found[13c] for the symmetric unit $[L'Mn(\mu\text{-}O)(\mu\text{-}CH_3CO_2)_2MnL']^{2+}$ for which a detailed analysis of the magnetic data gave J = +18 cm^{-1}, $D_1 = D_2$ = 3 cm^{-1}, $g_1 = g_2$ = 2.00 (E_1 and E_2 have been set to zero). For **1** a fit of the data yielded J = +14 cm^{-1}.

$[Fe^{III}(\mu\text{-}O)(\mu\text{-}CH_3CO_2)_2Fe^{III}]^{2+}$. The magnetic susceptibility was measured for the Fe^{III}_2 complex (**2**) as the perchlorate salt, and the results are represented in Figure 5. The product $\chi_M T$ per dinuclear unit decreases from 0.87 $cm^3\ mol^{-1}\ K$ at 292 K to 0.026 $cm^3\ mol^{-1}\ K$ at 7.9 K which is typical of antiferromagnetic coupling between the two high-spin Fe^{III} ions. The data could be fitted using the usual equation for the magnetic susceptibility of two coupled $S = {}^5/_2$ spins. The best fit was obtained with J = −207 cm^{-1} and g = 2.00 (fixed) with a small amount (1.25%) of paramagnetic impurity of spin $^5/_2$ and is shown in Figure 5.

$[Mn^{III}(\mu\text{-}O)(\mu\text{-}CH_3CO_2)_2Fe^{III}]^{2+}$. The magnetic susceptibilities of the $Mn^{III}Fe^{III}$ perchlorate salts **3** and **3a** are shown in Figure 6 as the product $\chi_M T$ as a function of T. $\chi_M T$ decreases with decreasing temperature in both cases. For **3**, $\chi_M T$ is equal to 1.45 $cm^3\ mol^{-1}\ K$ at 290.9 K and to 0.38 $cm^3\ mol^{-1}\ K$ at 19.4 K. For **3a**, $\chi_M T$ is equal to 1.57 $cm^3\ mol^{-1}\ K$ at 292 K and to 0.38 $cm^3\ mol^{-1}\ K$ at 15.9 K. These experimental data unambiguously indicate a strong antiferromagnetic coupling between the high-spin Mn^{III} and Fe^{III} ions, such that the ground states of both complexes have $S = {}^1/_2$. An analogous result had been found[15] for the symmetric species $[L'Fe(\mu\text{-}O)(\mu\text{-}CH_3CO_2)_2MnL']^{2+}$. To fit the data, we used the same spin Hamiltonian as in ref 15. The best fits gave J = −136 cm^{-1}, g_{Mn} = 1.98, g_{Fe} = 2.00 (fixed) for compound **3** and J = −126 cm^{-1}, g_{Mn} = 1.95, g_{Fe} = 2.00 (fixed) for **3a**. We do not consider the difference in the g_{Mn} values obtained in the two fits to be significant. We did not include zero field splitting effects since the ground state is an $S = {}^1/_2$ state

Table II. Summary of Crystal Data[a]

complex	3	4	5	6
formula	$[C_{19}H_{42}FeMnN_6O_5](ClO_4)_2 \cdot H_2O$	$[C_{19}H_{42}CrFeN_6O_5](PF_6)_2$	$[C_{19}H_{42}CrMnN_6O_5](ClO_4)_2$	$[C_{19}H_{42}CrMnN_6O_5](ClO_4)_3$
formula wt	762.3	832.3	740.4	839.9
crystal system	monoclinic	orthorhombic	monoclinic	monoclinic
space group	$C2/c$	$Pbca$	$P2_1/c$	$P2_1/m$
a, Å	23.929 (6)	18.951 (4)	11.146 (2)	11.332 (3)
b, Å	19.036 (5)	14.160 (5)	20.975 (4)	9.715 (1)
c, Å	16.701 (3)	24.619 (5)	13.563 (3)	16.180 (4)
β, deg	119.52 (1)		99.71 (2)	110.16 (1)
V, Å^3	6620.0	6606.4	3125.4	1672.1
Z	8	8	4	2
d_{calc}, g/cm^3	1.530	1.674	1.573	1.668
radiation (Mo Kα), Å	0.71073	0.71073	0.71073	0.71073
μ(Mo Kα), cm^{-1}	10.3	9.6	9.65	10.0
T, K	293 (1)	298 (1)	296 (1)	295 (1)
transm coeff	0.98–0.99	0.61–0.73	0.59–0.73	0.86–0.98
total reflcns measd	6213	7481	8503	4235
no. of indep observatns ($I > 2.0\sigma(I)$)	3866	2533	4543	3793
no. of var refined	283	320	284	230
R	0.091	0.081	0.078	0.085
R_w	0.081	0.072	0.069	0.0745

[a] Calculations were carried out with the SHELXTL-PLUS (Nicolet 1988) program. The function minimized in the least-squares refinements was $\sum w(|F_o| - |F_c|)^2$ where $w = 1/(\sigma^2(F) + 0.0001F^2)$. The residuals are defined as $R = \sum(|F_o| - |F_c|)/\sum|F_o|$ and $R_w = \{\sum w(|F_o| - |F_c|)^2/\sum w|F_o|^2\}^{1/2}$.

Table III. Selected Bond Distances (Å) and Angles (deg) for $[L'Fe(O)(CH_3CO_2)_2MnL](ClO_4)_2 \cdot H_2O$ (3)

Fe1–O1	1.817 (7)	Fe1–O3	2.006 (7)
Fe1–O4	2.027 (9)	Fe1–N1	2.246 (11)
Fe1–N2	2.192 (9)	Fe1–N3	2.181 (10)
Mn1–O1	1.782 (6)	Mn1–O2	2.091 (6)
Mn1–O5	2.007 (10)	Mn1–N4	2.084 (9)
Mn1–N5	2.146 (12)	Mn1–N6	2.221 (8)
O2–C21	1.256 (12)	O3–C21	1.226 (14)
C21–C22	1.486 (15)	O4–C23	1.270 (12)
O5–C23	1.247 (17)	C23–C24	1.493 (20)
Fe1···Mn1	3.115 (3)		
O1–Fe1–O3	98.5 (3)	O1–Fe1–O4	98.8 (3)
O3–Fe1–O4	94.1 (3)	O1–Fe–N1	172.7 (3)
O3–Fe1–N1	85.8 (3)	O4–Fe1–N1	86.7 (4)
O1–Fe1–N2	95.2 (3)	O3–Fe1–N2	90.3 (3)
O4–Fe1–N2	164.6 (4)	N1–Fe1–N2	78.9 (4)
O1–Fe1–N3	95.2 (4)	O3–Fe1–N3	164.6 (3)
O4–Fe1–N3	90.8 (4)	N1–Fe1–N3	79.8 (4)
N2–Fe1–N3	81.4 (3)	O1–Mn1–O2	95.4 (2)
O1–Mn1–O5	97.0 (3)	O2–Mn1–O5	95.2 (3)
O1–Mn1–N4	175.7 (4)	O2–Mn1–N4	87.9 (3)
O5–Mn1–N4	85.4 (4)	O1–Mn1–N5	96.4 (4)
O2–Mn1–N5	89.1 (3)	O5–Mn1–N5	165.4 (3)
N4–Mn1–N5	80.9 (4)	O1–Mn1–N6	94.9 (3)
O2–Mn1–N6	166.2 (4)	O5–Mn1–N6	92.6 (4)
N4–Mn1–N6	81.3 (3)	N5–Mn1–N6	80.6 (4)
Fe1–O1–Mn1	119.9 (4)		

Table IV. Selected Bond Distances (Å) and Angles (deg) for $[LFe(O)(CH_3CO_2)_2CrL'](PF_6)_2$ (4)

Fe1–O1	1.792 (7)	Fe1–O2	2.040 (8)
Fe1–O4	2.047 (8)	Fe1–N4	2.200 (9)
Fe1–N5	2.202 (10)	Fe1–N6	2.241 (10)
Cr1–O1	1.798 (7)	Cr1–O3	1.969 (8)
Cr1–O5	1.991 (8)	Cr1–N1	2.106 (10)
Cr1–N2	2.159 (10)	Cr1–N3	2.116 (10)
C21–O22	1.499 (17)	C21–O2	1.236 (16)
C21–O3	1.256 (15)	C23–C24	1.492 (18)
C23–O4	1.249 (15)	C23–O5	1.238 (15)
Fe1···Cr1	3.126 (2)		
O1–Fe1–O2	98.8 (3)	O1–Fe1–O4	98.1 (3)
O2–Fe1–O4	92.4 (3)	O1–Fe1–N4	96.8 (3)
O2–Fe1–N4	93.4 (3)	O4–Fe1–N4	163.0 (3)
O1–Fe1–N5	96.9 (3)	O2–Fe1–N5	163.4 (3)
O4–Fe1–N5	90.6 (3)	N4–Fe1–N5	79.6 (4)
O1–Fe1–N6	174.3 (4)	O2–Fe1–N6	85.0 (3)
O4–Fe1–N6	85.8 (3)	N4–Fe1–N6	78.8 (4)
N5–Fe1–N6	78.9 (4)	O1–Cr1–O3	95.4 (3)
O1–Cr1–O5	95.4 (3)	O3–Cr1–O5	93.4 (3)
O1–Cr1–N1	91.1 (4)	O3–Cr1–N1	93.7 (4)
O5–Cr1–N1	169.9 (3)	O1–Cr1–N2	174.1 (4)
O3–Cr1–N2	87.4 (4)	O5–Cr1–N2	89.5 (4)
N1–Cr1–N2	83.6 (4)	O1–Cr1–N3	94.7 (4)
O3–Cr1–N3	169.5 (4)	O5–Cr1–N3	88.4 (3)
N1–Cr1–N3	83.4 (4)	N2–Cr1–N3	82.2 (4)
Fe1–O1–Cr1	121.1 (4)		

which is well separated from the excited states. Introduction of zero-field splitting effects in those excited states has a very minor effect on the powder susceptibility. Intermolecular interactions were not included since such an effect was not detected. Slight variations of the J values are observed between the three complexes; we believe that they correspond to real effects which might be due to the coordination of different capping ligands.

$[Cr^{III}(\mu\text{-}O)(\mu\text{-}CH_3CO_2)_2Fe^{III}]^{2+}$. The results of the magnetic susceptibility measurements on the $Cr^{III}Fe^{III}$ salt **4** are shown Figure 7 as the product $\chi_M T$ per dinuclear unit as a function of temperature. This quantity decreases from 1.20 cm^3 mol^{-1} K at 288.5 K to reach at 117 K a plateau at 1 cm^3 mol^{-1} K. This behavior is characteristic of a strong antiferromagnetic coupling between the Cr^{III} and Fe^{III} ions yielding a $S = 1$ ground state. We fitted those data with the simple expression 6

$$\chi_M = \frac{N\beta^2}{kT}g^2\left[\frac{2 + 10e^{2x} + 28e^{5x} + 60e^{9x}}{3 + 5e^{2x} + 7e^{5x} + 9e^{9x}}\right] \quad (6)$$

where $x = J/kT$. An excellent simulation was obtained with $J = -275$ cm^{-1} and $g = 2.0$ (Figure 7).

$[Cr^{III}(\mu\text{-}OH)(\mu\text{-}CH_3CO_2)_2Fe^{III}]^{3+}$. The protonated complex (**4H**) was studied too; at room temperature (293.1 K), the product $\chi_M T$ per dinuclear unit (Figure 7) is 4.05 cm^3 mol^{-1} K. This quantity decreases to 1.02 cm^3 mol^{-1} K at 16.5 K. This is again the behavior of an antiferromagnetically coupled pair. Equation 6 was used to fit the data, and J was calculated to be −43 cm^{-1}. The large decrease in the coupling parameter upon protonation of the oxo bridging ligand is not unusual and is related to the accompanying elongation of the M^{III}–O bonds. In the fitting procedure we did not include zero-field splitting effects or an intermolecular interaction since no manifestations of such effects were detectable in our experiments.

$[Cr^{III}(\mu\text{-}O)(\mu\text{-}CH_3CO_2)_2Mn^{III}]^{2+}$. The hexafluorophosphate salt of **5** was studied. The product $\chi_M T$ per dinuclear unit increases from 5.44 cm^3 mol^{-1} K at 293.4 K to 6.93 cm^3 mol^{-1} K at 19.3 K. (Data not shown.) This is typical of a ferromagnetic coupling between the Cr^{III} and Mn^{III} ions. The expected value of $\chi_M T$ = 7.875 cm^3 mol^{-1} K for a spin $S = {}^7/_2$ ground state is not reached which is indicative of intermolecular antiferromagnetic interactions

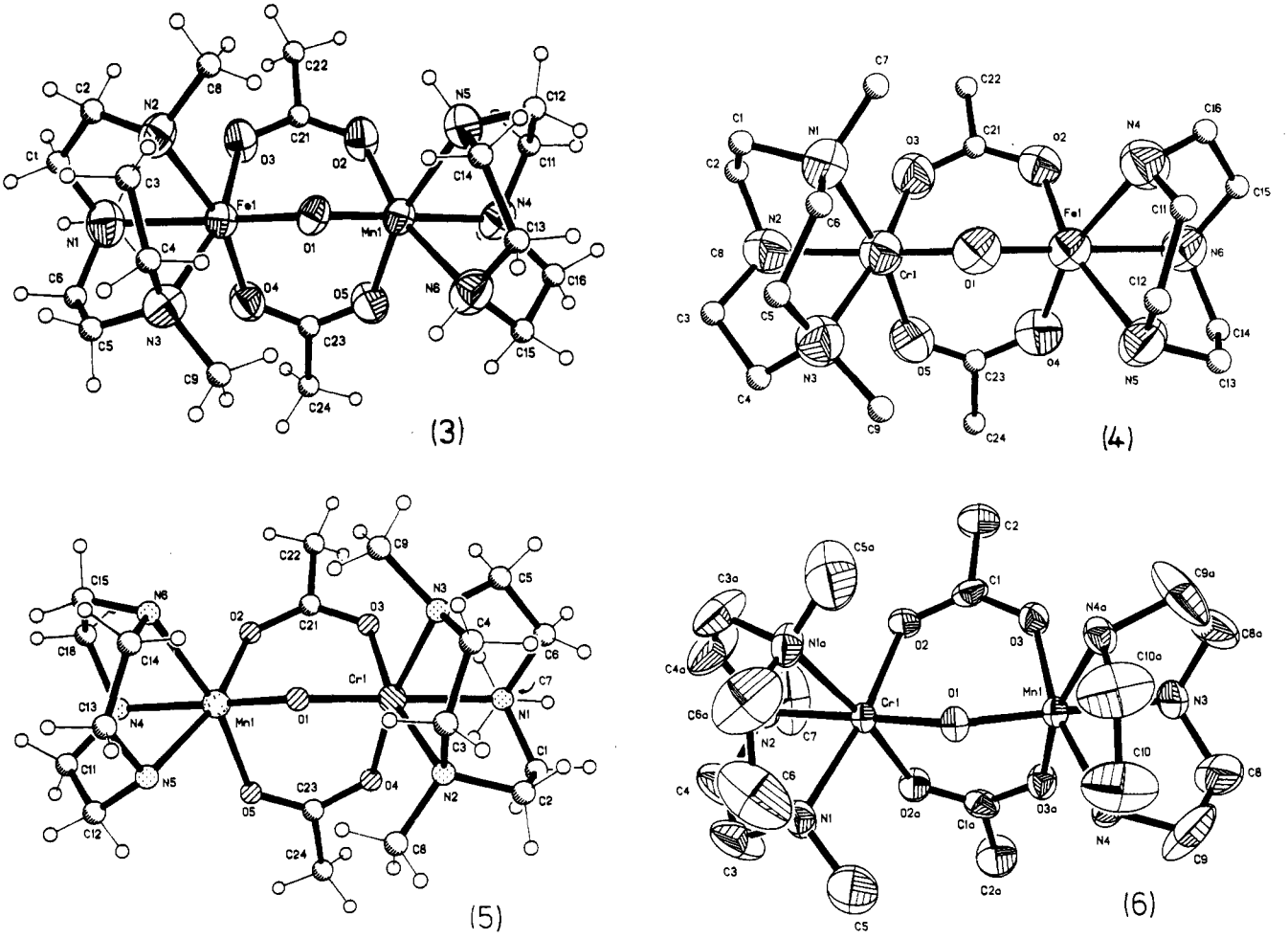

Figure 1. Structures of the cations and their respective atom labeling scheme.

Table V. Selected Bond Distances (Å) and Angles (deg) for $[LMn(O)(CH_3CO_2)_2CrL']$$(ClO_4)_2$ (**5**)

Cr1–O1	1.854 (5)	Cr1–O3	1.967 (5)
Cr1–O4	1.967 (6)	Cr1–N1	2.157 (7)
Cr1–N2	2.115 (7)	Cr1–N3	2.097 (8)
Mn1–O1	1.763 (5)	Mn1–O2	2.072 (5)
Mn1–O5	2.080 (6)	Mn1–N4	2.108 (7)
Mn1–N5	2.212 (6)	Mn1–N6	2.206 (7)
C21–C22	1.505 (11)	C21–O2	1.261 (10)
C21–O3	1.244 (10)	C23–C24	1.498 (14)
C23–O4	1.265 (11)	C23–O5	1.240 (11)
Cr1···Mn1	3.147 (2)		
O1–Cr1–O3	96.9 (2)	O1–Cr1–O4	96.6 (2)
O3–Cr1–O4	95.2 (2)	O1–Cr1–N1	173.2 (3)
O3–Cr1–N1	87.7 (2)	O4–Cr1–N1	88.0 (3)
O1–Cr1–N2	91.8 (2)	O3–Cr1–N2	167.5 (3)
O4–Cr1–N2	92.7 (3)	N1–Cr1–N2	82.9 (3)
O1–Cr1–N3	92.6 (3)	O3–Cr1–N3	88.1 (3)
O4–Cr1–N3	169.8 (3)	N1–Cr1–N3	82.5 (3)
N2–Cr1–N3	82.6 (3)	O1–Mn1–O2	97.6 (2)
O1–Mn1–O5	96.0 (2)	O2–Mn1–O5	93.7 (2)
O1–Mn1–N4	174.2 (2)	O2–Mn1–N4	86.5 (2)
O5–Mn1–N4	87.8 (3)	O1–Mn1–N5	94.3 (2)
O2–Mn1–N5	166.0 (2)	O5–Mn1–N5	92.3 (2)
N4–Mn1–N5	81.1 (3)	O1–Mn1–N6	95.5 (3)
O2–Mn1–N6	91.2 (2)	O5–Mn1–N6	166.8 (3)
N4–Mn1–N6	80.2 (3)	N5–Mn1–N6	80.3 (3)
Cr1–O1–Mn1	120.9 (2)	C22–C21–O2	118.1 (7)
C22–C21–O3	115.6 (7)	O2–C21–O3	126.2 (7)

Table VI. Selected Bond Distances (Å) and Angles (deg) for $[L'Cr(O)(CH_3CO_2)_2MnL](ClO_4)_3$ (**6**)

Mn1···Cr1	3.186 (2)	Cr1–O1	1.882 (8)
Mn1–O3	1.890 (6)	Cr1–N1	2.100 (7)
Mn1–N4	2.038 (7)	Cr1–O2	1.973 (6)
Mn1–O1	1.743 (5)	Cr1–N2	2.117 (10)
Mn1–N3	2.079 (7)		
Mn1–O1–Cr1	123.0 (4)	O1–Mn1–N3	176.5 (4)
O1–Mn1–O3	97.0 (2)	O3–Mn1–O3a	96.4 (3)
O1–Mn1–O4	94.3 (2)	O3–Mn1–N4	166.9 (2)
O3–Mn1–N3	85.3 (2)	N3–Mn1–N4	83.1 (3)
O3–Mn1–N4a	88.6 (3)	O1–Cr1–O2	93.0 (2)
N4–Mn1–N4a	84.1 (3)	O1–Cr1–N2	177.0 (3)
O1–Cr1–N1	93.9 (3)	O2–Cr1–N1	171.9 (3)
O2–Cr1–O2a	92.5 (2)	O2–Cr1–N2	89.0 (2)
O2–Cr1–N1a	91.2 (3)	N1–Cr1–N2	83.9 (3)
N1–Cr1–N1a	84.3 (3)		

and/or zero-field splitting effects in the ground state. We estimated J by taking data points above T = 150 K and fitted those values by using a simple Heisenberg law to obtain $J = +10$ cm^{-1}.

$[Cr^{III}(\mu\text{-}O)(\mu\text{-}CH_3CO_2)_2Mn^{IV}]^{3+}$. The hexafluorophosphate salt of **6** was studied. The product $\chi_M T$ per dinuclear unit increases from 0.28 cm^3 mol^{-1} K at 62.7 K to 1.86 cm^3 mol^{-1} K at 290.9 K (Figure 8). This demonstrates antiferromagnetic coupling between these two d^3 ions. The data were fitted with a simple Heisenberg law and $J = -87$ cm^{-1} with $g = 1.97$ gave an excellent simulation; this g value agrees, within the experimental accuracy, with the expected value for d^3 ions.

$[Cr^{III}(\mu\text{-}O)(\mu\text{-}CH_3CO_2)_2V^{III}]^{2+}$. The perchorate salt of **7** was studied over the temperature range 4.2–293 K. The product $\chi_M T$ per dinuclear unit is constant at 4.1 cm^3 mol^{-1} K, indicative of a very strong ferromagnetic coupling, $J > +200$ cm^{-1}, between the Cr^{III} and the V^{III} ions. An $S = {}^5/_2$ ground state is observed even at room temperature.

$[Fe^{III}(\mu\text{-}O)(\mu\text{-}CH_3CO_2)_2Mn^{IV}]^{3+}$. The temperature-dependent magnetic susceptibilities of the isomers **8** and **8a** were studied. All measurements showed substantial amounts of paramagnetic impurities so that a good fit could not be obtained. Nevertheless

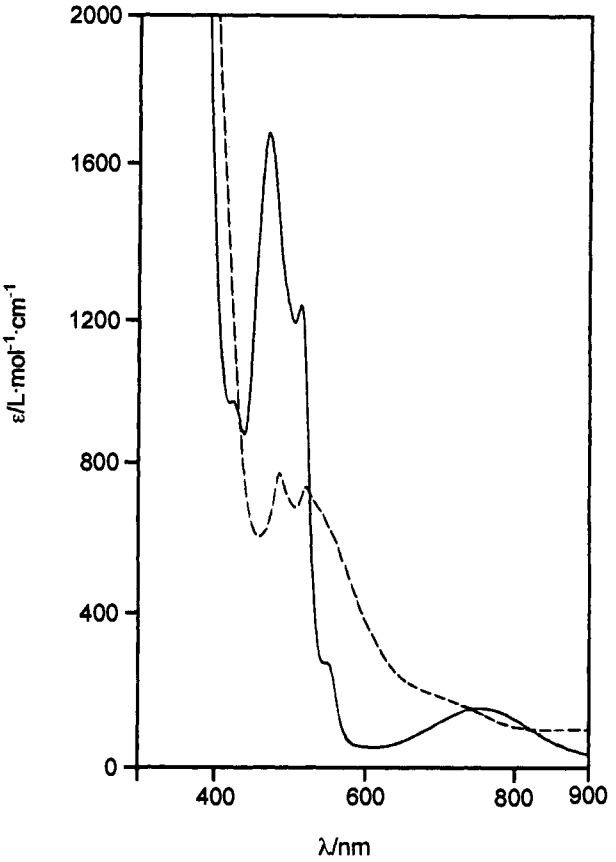

Figure 2. Electronic spectra of $[L'Mn^{III}O(CH_3CO_2)_2Mn^{III}L]^{2+}$ (**1**) (--) and $[L'Fe^{III}O(CH_3CO_2)_2Fe^{III}L]^{2+}$ (**2**) (—) in acetonitrile, T = 20 °C.

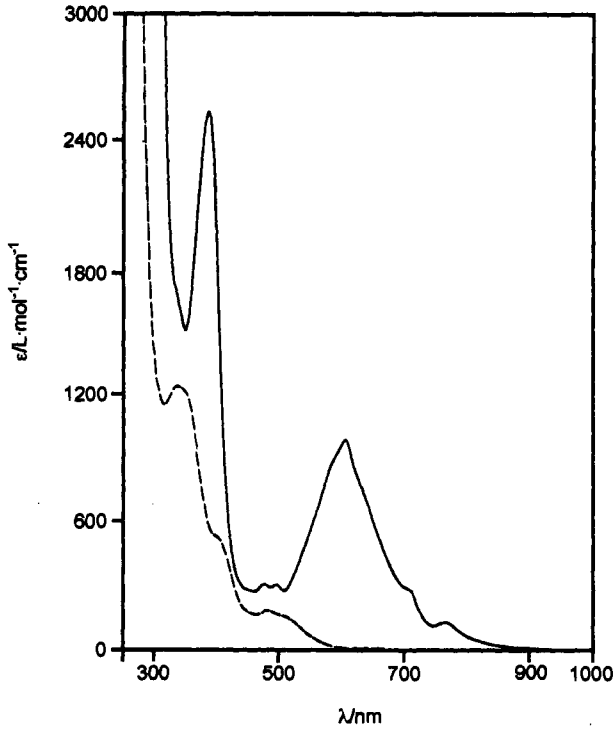

Figure 3. Electronic spectra of $[LFe^{III}O(CH_3CO_2)_2Cr^{III}L']^{2+}$ (**4**) (—) and $[LFe^{III}(OH)(CH_3CO_2)_2Cr^{III}L']^{3+}$ (**4H**) (--) in acetonitrile, T = 20 °C.

an antiferromagnetic behavior was observed corresponding to the effects in $Fe^{III}Cr^{III}$ (**4**) which is also a d^5d^3 system.

Discussion

Magnetic Properties. The magnetic interactions in the $[M^1(\mu\text{-}O)(\mu\text{-}CH_3CO_2)_2M^2]^{2+}$ units together with previously reported

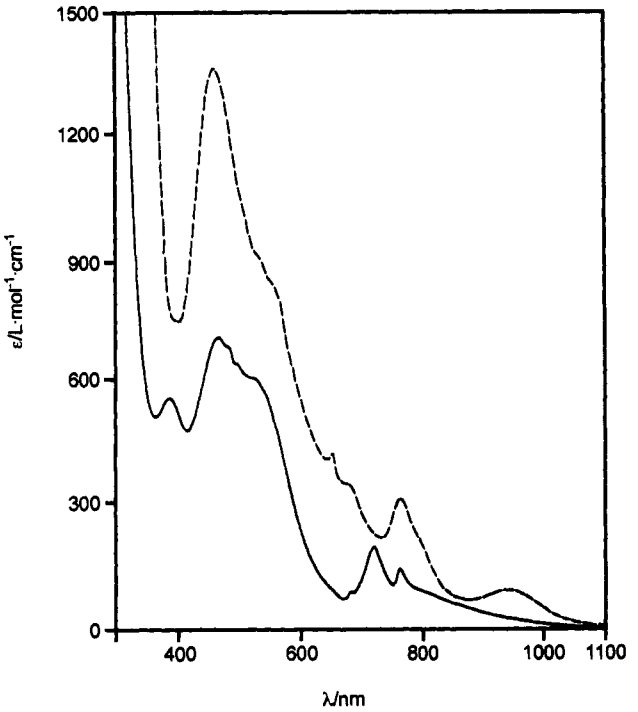

Figure 4. Electronic spectra of $[LMn^{III}O(CH_3CO_2)_2Cr^{III}L']^{2+}$ (**5**) (—) and $[LMn^{IV}O(CH_3CO_2)_2Cr^{III}L']^{3+}$ (**6**) (--) in acetonitrile, T = 20 °C.

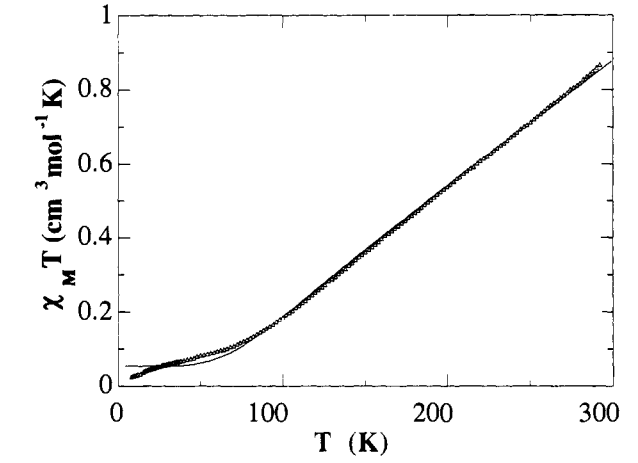

Figure 5. Plot of $\chi_M T$ vs T for a powder sample of $[LFeO(CH_3CO_2)_2FeL'](ClO_4)_2 \cdot H_2O$. The solid line represents the data fit to the isotropic Heisenberg model for electron exchange (see text).

results of the homodinuclear species are summarized in Table VIII and in matrix form in Table IX for the following discussion. A striking feature is the range of observed values considering the structural similarity of the complexes.

We begin with some general comments on electron exchange theory. Then we present a simple model to explain the main features of the magnetic properties of this series of compounds and, finally, extended Hückel calculations of molecular orbitals are used to refine this model. The influence of the M–O–M angle on the magnetic coupling is investigated, and, finally, a tentative hypothesis for the ferromagnetic coupling in V^{III}–O–V^{III} systems is introduced.

The theory of electron exchange between metallic ions in polynuclear complexes is well established.[25-28,36] This phenomenon

(25) Anderson, P. W. In *Magnetism*; Rado, G. T., Suhl, H., Eds.; Academic Press: New York, 1963; Vol. 1, Chapter 2.
(26) Hay, P. J.; Thibeault, J. C.; Hoffmann, R. *J. Am. Chem. Soc.* **1975**, *97*, 4884.
(27) *Magneto-Structural Correlations in Exchange Coupled Systems*; Willet, R. D., Gatteschi, D., Kahn, O., Eds.; D. Reidel: 1985.

Table VII. Electronic Spectra of Complexes[a]

complex	M^1 M^2	d^m d^n	λ, nm (ε, L mol^{-1} cm^{-1})
1	Mn^{III} Mn^{III}	4 4	246 (1.1 × 10^4), 304 (1.2 × 10^4), 481 (770), 521 (740), 680 sh (200)
2	Fe^{III} Fe^{III}	5 5	241 (1.3 × 10^4), 270 sh (6.5 × 10^3), 340 (8 × 10^3), 423 (960), 472 (1.7 × 10^3), 515 (1.2 × 10^3), 550 sh (270), 757 (150)
3	Mn^{III} Fe^{III}	4 5	293 (3.7 × 10^3), 428 (980), 471 (830), 520 sh (490), 580 sh (300), 1150 (40)
3a	Mn^{III} Fe^{III}	4 5	265 (5.7 × 10^3), 338 (4.4 × 10^3), 418 (1.1 × 10^3), 455 (720), 465 sh (700), 530 (350), 570 (290), 1150 (40)
4	Cr^{III} Fe^{III}	3 5	330 sh (1.7 × 10^3), 382 (2.6 × 10^3), 477 (310), 496 (310) 590 sh (900), 605 (1.0 × 10^3), 630 sh (800), 710 sh (290), 765 (130)
4H	Cr^{III} Fe^{III}	3 5	338 (1.3 × 10^3), 350 sh (1.2 × 10^3), 400 sh (560), 480 (190) 520 sh (160), 650 (21), 685 (15), 710 sh (10), 765 (6)
5	Cr^{III} Mn^{III}	3 4	389 (560), 469 (710), 485 (690), 500 (640), 525 sh (610), 540 sh (590), 640 sh (110), 686 (90), 723 (200), 765 (150)
6	Cr^{III} Mn^{IV}	3 3	462 (1.4 × 10^3), 530 sh (900), 560 sh (820), 656 (420) 680 (350), 767 (320), 800 sh (220), 940 (100)
7	Cr^{III} V^{III}	3 2	260 sh (2.9 × 10^3), 378 (2.7 × 10^3), 592 (360)
8	Fe^{III} Mn^{IV}	5 3	320 sh (9 × 10^3), 390 sh (4.9 × 10^3), 460 sh (1.3 × 10^3) 515 sh (900), 560 (600), 620 sh (510), 740 sh (200)
8a	Fe^{III} Mn^{IV}	5 3	290 (1.3 × 10^4), 315 (1.4 × 10^4), 380 sh (5.2 × 10^3), 480 sh (880), 515 sh (660), 560 sh (550), 620 sh (440), 735 sh (170)

[a] Measured in CH_3CN at 20 °C.

Table VIII. Spin Exchange Coupling Constants and Spin Values for the Ground State of $[MO(CH_3CO_2)_2M']^{n+}$ Complexes

	compds	J (cm^{-1}) ($\mathcal{H} = -JS_A \cdot S_B$)	spin of the ground state	ref
1	$[LMnO(CH_3CO_2)_2MnL'](ClO_4)_2 \cdot H_2O$	+14	4	this work
2	$[L'FeO(CH_3CO_2)_2FeL](ClO_4)_2 \cdot H_2O$	−207	0	this work
3	$[L'FeO(CH_3CO_2)_2MnL](ClO_4)_2 \cdot H_2O$	−136	1/2	this work
3a	$[L'MnO(CH_3CO_2)_2FeL](ClO_4)_2 \cdot H_2O$	−126	1/2	this work
4	$[L'CrO(CH_3CO_2)_2FeL](ClO_4)_2 \cdot H_2O$	−275	1	this work
4H	$[L'CrOH(CH_3CO_2)_2FeL](ClO_4)_3 \cdot 2H_2O$	−43	1	this work
5	$[L'CrO(CH_3CO_2)_2MnL](PF_6)_2$	+10	7/2	this work
6	$[L'CrO(CH_3CO_2)_2MnL](PF_6)_3$	−87	0	this work
7	$[L'CrO(CH_3CO_2)_2VL](ClO_4)_2$	F[a]	5/2	this work
	$[L'CrO(CH_3CO_2)_2CrL'](BPh_4)_2$	−64	0	48
	$[L'VO(CH_3CO_2)_2VL']^{2+}$	F[a]	2	18a
	$[L'TiO(PhCO_2)_2TiL']^{2+}$	AF[b]	0	17

[a] F, ferromagnetic. [b] AF, antiferromagnetic.

Table IX. Magnetic Coupling Properties[a] for $[M^{III}O(CH_3CO_2)_2M'^{III}]^{2+}$ Complexes

	Ti(III)	V(III)	Cr(III)	Mn(III)	Fe(III)
Ti(III)	AF				
V(III)		F	F		
Cr(III)			−64	+10	−275
Mn(III)				+18	−136
				+14	−126
					−145
Fe(III)					−207

[a] J values in cm^{-1}, AF antiferromagnetic, F ferromagnetic.

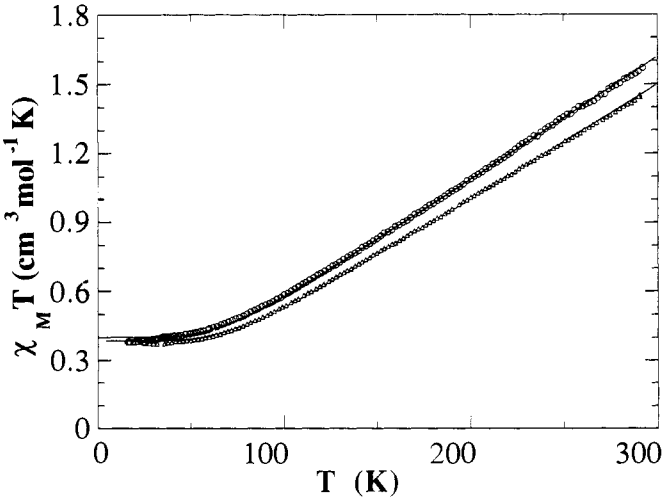

Figure 6. Plots of $\chi_M T$ vs T for powder samples of $[L'MnO(CH_3CO_2)_2FeL](ClO_4)_2 \cdot H_2O$ (○) and of $[L'FeO(CH_3CO_2)_2MnL](ClO_4)_2 \cdot H_2O$ (△). The solid lines represent the data fits to the isotropic Heisenberg model for electron exchange (see text).

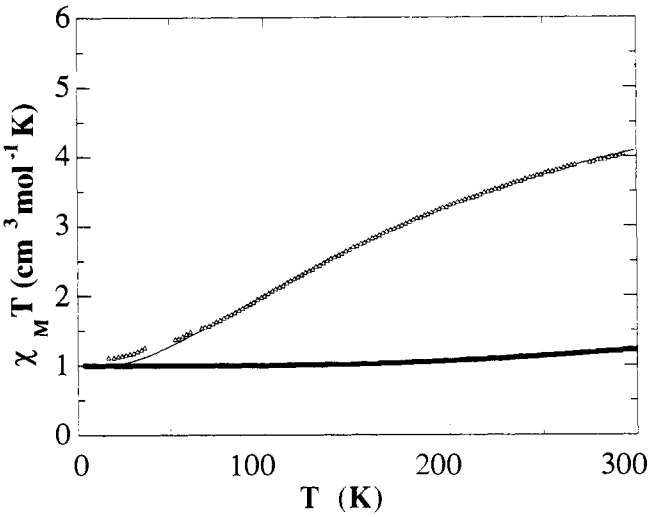

Figure 7. Plots of $\chi_M T$ vs T for powder samples of $[L'CrO(CH_3CO_2)_2FeL](ClO_4)_2 \cdot H_2O$ (thick solid line) and of $[L'Cr(OH)(CH_3CO_2)_2FeL](ClO_4)_3 \cdot 2H_2O$ (△). The solid lines represent the data fits to the isotropic Heisenberg model for electron exchange (see text).

is expressed in the form of the Heisenberg Hamiltonian $\mathcal{H} = -JS_A \cdot S_B$ where S_i is the spin of ion i in its ground state and J is the energy of interaction. This Hamiltonian comes from first- and second-order perturbational treatment of the interaction between the two ions. It clearly assumes that the interaction is weak since the spin of the ground states of the individual ions retain a meaning. The electron exchange situation and chemical

(28) *Electron Paramagnetic Resonance of Exchange Coupled Systems*; Bencini, A., Gatteschi, D., Eds.; Springer-Verlag: Berlin, 1990.

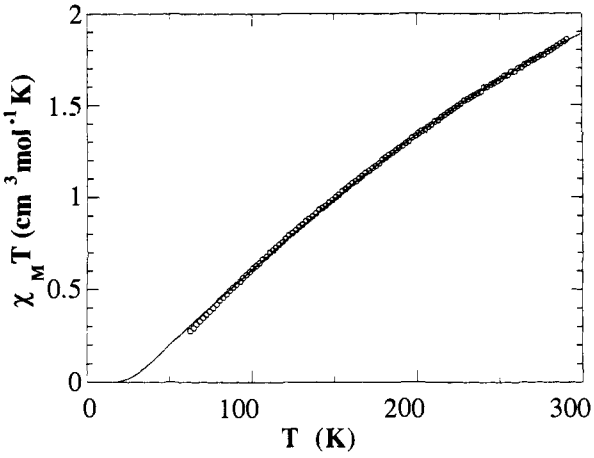

Figure 8. Plots of $\chi_M T$ vs T for a powder sample of $[L'CrO(CH_3CO_2)_2MnL](PF_6)_3$. The solid line represents the data fits to the isotropic Heisenberg model for electron exchange (see text).

bonding[29,30] are limiting forms of the same basic phenomenon: electrostatic interactions between electrons and electrons and electrons and nuclei.

In the simplest treatments,[25-28] only the *half occupied* orbitals on each ion in its ground state are considered. The parameter J can be related to the individual J_{ij} interactions between orbitals i of ion A and orbitals j of ion B as in eq 7

$$J = \frac{1}{n_A n_B} \sum_{i,j} J_{ij} \tag{7}$$

where n_i is the number of unpaired electrons on ion i. The following scheme illustrates this point.

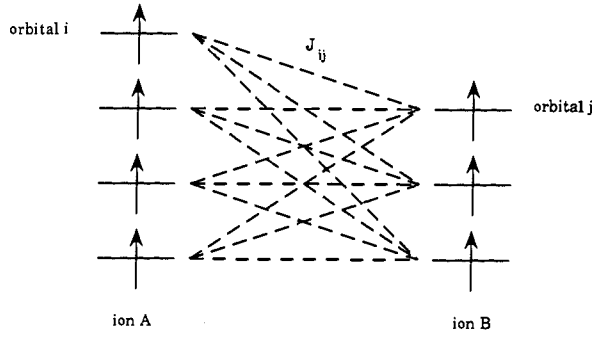

As proposed by Anderson[25] for infinite systems and then applied to clusters by Hoffmann[26] and Kahn,[31] the orbitals considered are not pure metal orbitals: they contain ligand contributions and must describe adequately the unpaired electrons around each center.

In these treatments J_{ij} contains two contributions of opposite sign, eq 8. There is general agreement on the expression of the

$$J_{ij} = J_{ij}^{F} + J_{ij}^{AF} \tag{8}$$

positive term J_{ij}^{F} as in eq 9

$$J_{ij}^{F} = 2k_{ij} \tag{9}$$

where k_{ij} is the intercenter exchange integral, eq 10

$$k_{ij} = \int a_i^*(1) b_j^*(2) (1/r_{12}) a_i(2) b_j(1) dv_1 dv_2 \tag{10}$$

On the other hand, different expressions can be found for the negative term J_{ij}^{AF} that corresponds to the antiferromagnetic coupling. For homodinuclear species with high symmetry Anderson[25] and Hoffmann[26] built orthogonal localized orbitals a_i and b_i from molecular orbitals ϕ_{ui} and ϕ_{gi}, such that $a_i = (\phi_{ui} + \phi_{gi})/\sqrt{2}$ and $b_i = (\phi_{ui} - \phi_{gi})/\sqrt{2}$. In these cases only J_{ii}^{AF} contributions exist, and eq 11 was proposed

$$J_{ii}^{AF} = -\frac{4\beta_{ii}^2}{U} \tag{11}$$

where β_{ij} is the energy of interaction between orbitals a_i and b_i (transfer integral or resonance integral in Hückel theory of molecular orbitals), and U is the cost in energy for transferring one electron from site A to site B or vice versa. Interesting features of this approach are that localized orbitals are well defined mathematically and that in formal calculations no overlap integrals occur. There are negative aspects of this approach. The localized orbitals are not strictly localized since in order to be orthogonal to each other they must have tails on the other center, which obscures the physical meaning of these orbitals. In addition although the definition of localized orbitals is clear for molecules with a symmetry high enough to avoid mixing of different MOs, it does not seem to be adapted to low symmetry systems in which this mixing is extensive.

Kahn[31] has developed other calculations with strictly localized orbitals which are not necessarily orthogonal to each other. In these circumstances eq 12 holds

$$J_{ij}^{AF} = 4t_{ij}S_{ij} \tag{12}$$

where S_{ij} is the overlap between orbitals a_i and b_j, and t_{ij} is the transfer integral defined as in eq 13

$$t_{ij} = \beta_{ij} - \frac{\alpha_{Ai} + \alpha_{Bj}}{2} S_{ij} \tag{13}$$

In this definition, one has eqs 14 and 15

$$\beta_{ij} = \int a_i^*(1) h(1) b_i(1) dv_1 \tag{14}$$

$$\alpha_{Ai} = \int a_i^*(1) h(1) a_i(1) dv_1 \tag{15}$$

where β_{ij} is the resonance integral and α_{Ai} is the energy of orbital a_i. One interesting aspect of this approach is that the orbitals are strictly localized and are close to chemical intuition about polynuclear complexes made up of the juxtaposition of mononuclear fragments. The mutual overlap will govern the intensity of the resonance integral through the Mulliken approximation eq 16.

$$\beta_{ij} = K\frac{\alpha_{Ai} + \alpha_{Bj}}{2} S_{ij} \tag{16}$$

Orbitals orthogonal by symmetry will have evidently $\beta_{ij} = S_{ij} = 0$ and will not contribute to antiferromagnetism (as in chemical bonding). This approach is not restricted to homopolynuclear complexes of high symmetry. One drawback of this approach is that it considers only ground-state configurations and this could prove inadequate for some systems: Although the excited-state configurations can be high in energy, they can nevertheless play a role in the small energy gaps we are considering.

Both approaches agree that antiferromagnetism has its origin in the resonance integral β_{ij}: the greater the interaction the stronger the antiferromagnetism. There are nevertheless more than simple mathematical differences between the two approaches. In the Anderson–Hoffmann approach, antiferromagnetism arises from what appears to be a metal–metal charge transfer: for instance a Fe^{III}–O–Fe^{III} unit will be antiferromagnetically coupled due to mixing of the ground-state oxidation-state distribution with the excited-state Fe^{II}–O–Fe^{IV} oxidation-state distribution. In Kahn's treatment, the Fe^{II}–O–Fe^{IV} oxidation-state distribution is considered to be at such a high energy that this mixing is negligible; in Kahn's approach antiferromagnetic coupling in a Fe^{III}–O–Fe^{III} unit arises solely from overlap between localized orbitals. Detailed comparison of these two approaches can be found in ref 32.

(29) Dubicki, L.; Krausz, E.; Stranger, R.; Smith, P. W.; Tanabe, Y. *Inorg. Chem.* **1987**, *26*, 2247–2254.
(30) Blondin, G.; Girerd, J.-J. *Chem. Rev.* **1990**, *90*, 1359.
(31) Kahn, O. in ref 27.

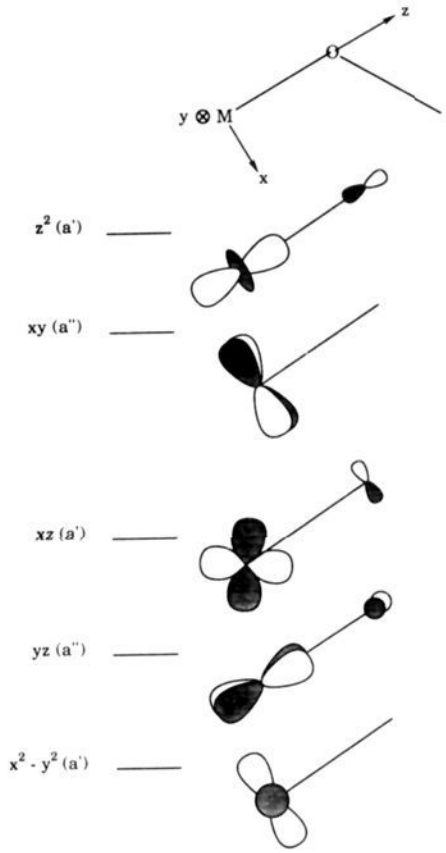

Figure 9. Local orbitals around one metal ion in the $[MO(CH_3CO_2)_2M']^{2+}$ unit.

The question as to which of these two approaches is best has not been answered. It may well depend on the systems studied: for systems with the site-to-site charge-transfer excitation low in energy, the Anderson–Hoffmann model could be a very good description; for others with very high excitation energies, the Kahn description could be more relevant.

Here we use a slightly different treatment. We start by using localized orbitals as defined by common chemical knowledge on mononuclear complexes (Kahn's method). Clearly, in general those orbitals have no reason to be orthogonal. This allows us to discuss the overlaps between these orbitals. But in formal calculations we consider that these orbitals are orthogonal. This enables us to treat multiconfigurational problems without using complicated formulas in which overlaps would have to be included explicitly. It means that we use eq 11 or a generalized one for heterodinuclear complexes eq 17

$$J_{ij}^{AF} = -2\beta_{ij}^2\left[\frac{1}{\Delta_{ij}} + \frac{1}{\Delta_{ji}}\right] \qquad (17)$$

where Δ_{ij} is the cost in energy to transfer an electron from a_i to b_j and vice versa for Δ_{ji}.

We emphasize that we have discussed above the simplest approach to electron exchange. In particular, we have assumed that the bridging ligand orbitals are low enough in energy that they do not participate by themselves but only as perturbations on the metal orbitals. This can be invalid for some systems. For instance in the best calculation available for the J coupling in $Cu_2(CH_3CO_2)_4 \cdot 2H_2O$, Malrieu et al.[33] have shown that processes implicating the acetato orbitals (double spin polarization in particular) have to be considered. Double spin polarization has also been indicated in copper azido systems.[34,35]

Magnetic coupling effects can come from interactions other than those between half-filled orbitals. It has been proposed that interactions between half-filled orbitals on one metal and empty orbitals on the other metal can contribute to ferromagnetic coupling.[36] We suggest in what follows that the observed ferromagnetism in the Mn^{III}–O–Mn^{III} species is due to such an interaction.

Are the magnetic interactions so complicated that a simple rationalization is not possible? Several previous studies[26,27] give us confidence that this is not so and that focusing on the β_{ij} can indeed help in understanding the influence of geometry in a series of structurally related compounds. Concerning this point Daudey[35] has shown how rigorous theoretical calculations can agree qualitatively with elementary ones of the type we have performed in this study. This is due to the fact that the β_{ij} terms are quite sensitive to geometry changes.

A Simple Approach: The Importance of the "Crossed Interaction". In the following we use metal centered orbitals but include participation of the ligand orbitals. We assume that the most important bridging ligand is the oxo group since it enforces the shortest metal-to-ligand bond distances. We do not assign an active role to the oxo group orbitals since they are much lower in energy than the metal orbitals. The acetato bridging ligand orbitals may participate in the magnetic coupling, but we assume that this will be to a much smaller extent than the oxo ligand orbitals.

Let us consider the following idealized C_{2v} geometry for the homodinuclear compounds of this study.

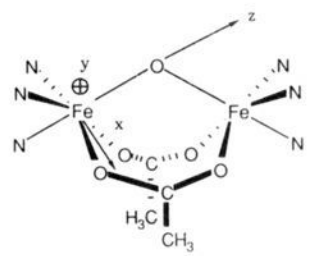

The first step is to qualitatively identify the local orbitals. These are illustrated in Figure 9. Both metal ions in the complex have a compressed octahedral geometry, the metal–oxo distance is the shortest and the corresponding interaction is the strongest. The symmetry is lower than D_{4h}; it is only C_s. The local orbitals are labeled by the irreducible representations of this symmetry group.

Considering the orbitals on each center it is clear that the a′ orbitals of center A overlap with the a′ orbitals of center B (likewise for the a″ family). The following resonance integrals can therefore be different from zero: $\beta_{z^2-z^2}$, β_{z^2-xz}, β_{xz-z^2}, $\beta_{z^2-(x^2-y^2)}$, $\beta_{(x^2-y^2)-z^2}$, β_{xz-xz}, $\beta_{xz-(x^2-y^2)}$, $\beta_{(x^2-y^2)-xz}$, $\beta_{(x^2-y^2)-(x^2-y^2)}$ for the a′ family and β_{xy-xy}, β_{xy-yz}, β_{yz-xy}, β_{yz-yz} for the a″ family.

We will use the term "crossed interactions" for those orbital interactions β_{ij} where $i \neq j$. Note that in a heterodinuclear species $\beta_{ij} \neq \beta_{ji}$. In high symmetry systems β_{ij} will in general vanish because a_i and b_j orbitals have different symmetries. Here in a low symmetry situation β_{ij} can be nonzero. This remark is at the heart of our proposals to interpret the magnetic properties of the bent M–O–M units.

Comparison of the overlaps between the different localized orbitals suggests that some of these interactions will be more important than others. Inspection of the following schemes suggests that the largest overlaps are S_{yz-yz} and S_{z^2-xz}.

(32) Girerd, J.-J.; Journaux, Y.; Kahn, O. *Chem. Phys. Lett.* **1981**, *82*, 534–538.

(33) de Loth, P.; Cassoux, P.; Daudey, J. P.; Malrieu, J. P. *J. Am. Chem. Soc.* **1981**, *103*, 4007–4016.

(34) Charlot, M.-F.; Kahn, O.; Chaillet, M.; Larrieu, C. *J. Am. Chem. Soc.* **1986**, *108*, 2574–2581.

(35) Daudey, J. P.; de Loth, P.; Malrieu, J. P. in ref 27.

(36) Goodenough, J. B. *Magnetism and the Chemical Bond*; Interscience Publishers: New York, 1963. See, also: the review by Ginsberg, A. P. *Inorg. Chim. Acta* **1971**, 45–68.

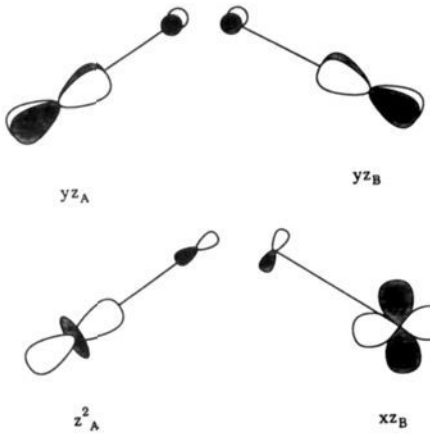

At small M–O–M angles $S_{z^2-z^2}$ is not large as may be deduced from the following scheme:

If $2s_o$ and $2p_o$ mixing is allowed for, this overlap is even smaller. In the case of Fe^{III}–O–Fe^{III}, the leading orbital interactions will be β_{yz-yz} and $\beta_{xz-z^2} = \beta_{z^2-xz}$. Using eq 17 we see that these orbital interactions will lead to antiferromagnetic interactions $J_{z^2-xz}{}^{AF}$, $J_{xz-z^2}{}^{AF}$ and $J_{yz-yz}{}^{AF}$ (Figure 10).

Going now to the Mn^{III}–O–Mn^{III} pair, how can we understand the very small anti- or even ferromagnetic coupling observed? Certainly, the $J_{z^2-xz}{}^{AF}$, $J_{xz-z^2}{}^{AF}$ pathways disappear since the z^2 orbitals are empty, but the $J_{yz-yz}{}^{AF}$ antiferromagnetic pathway remains and it is a well-documented observation that, in general, when there are overlapping orbitals, the overall coupling is antiferromagnetic. The counterpoint of this observation is that an efficient strategy to have ferromagnetic coupling is to build systems with orbitals orthogonal by symmetry.[37,38]

We propose to explain our experimental observation of ferromagnetic coupling in several complexes of this series by reviving the somewhat neglected idea that strong overlap between one empty orbital and one half-filled orbital can lead to ferromagnetic coupling. This introduces a source of ferromagnetism other than the exchange integrals of eq 9 and allows one to understand that despite the existence of the antiferromagnetic pathway $J_{yz-yz}{}^{AF}$, the $[Mn^{III}(\mu\text{-}O)(\mu\text{-}CH_3CO_2)_2Mn^{III}]^{2+}$ unit is not strongly antiferromagnetically coupled.

The following simple illustration can be given for this ferromagnetic coupling by crossed interaction. Let us consider that a crossed interaction β_{12} exists between two centers each one containing only one unpaired electron. For simplicity β_{11} and β_{22} are assumed to be zero.

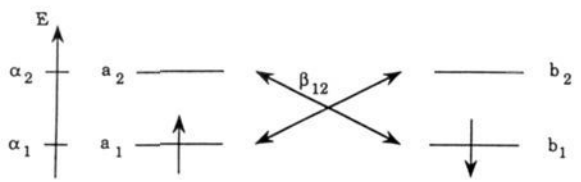

When β_{12} is neglected, the ground subspace corresponding to the configuration a_1b_1 is degenerate, but the excited subspace

(37) Pei, Y.; Journaux, Y.; Kahn, O. *Inorg. Chem.* **1989**, *28*, 100–103.
(38) Journaux, Y.; Kahn, O.; Zarembovitch, J.; Galy, J.; Jaud, J. *J. Am. Chem. Soc.* **1983**, *105*, 7585–7591.

Table X. Metal d Orbital Composition of the Five Metal d Rich Orbitals for the Fragment N_5FeO

	z^2_A (a′)	xy_A (a″)	yz_A (a″)	xz_A (a′)	$(x^2-y^2)_A$ (a′)
d_{z^2}	0.9222	0	0	0	−0.0676
d_{xy}	0	0.955	0	0	0
d_{yz}	0	0	0.9416	0	0
d_{xz}	0	0	0	0.9417	0
$d_{x^2-y^2}$	0.0676	0	0	0	0.9964

corresponding to the metal–metal charge-transfer configurations a_1a_2 or b_1b_2 is split due to intraatomic exchange K (see scheme).

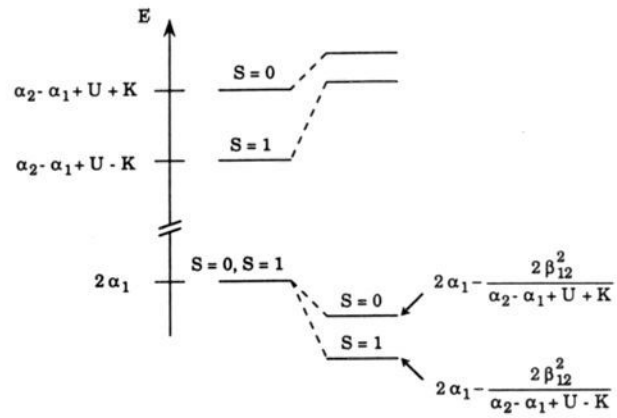

The interaction β_{12} mixes the ground subspace and the excited one in such a way that the degeneracy of the ground subspace is lifted to give a triplet ground state, the stabilization of which versus the singlet is[36] as in eq 18.

$$\frac{4\beta_{12}^2}{(\alpha_2 - \alpha_1 + U)^2}K \qquad (18)$$

The triplet is the ground state because the coupling matrix element is the same for the triplet and the singlet, but the excited triplet is lower in energy than the excited singlet. This ferromagnetic contribution is smaller than the usual AF one by a ratio $K/(\alpha_2 - \alpha_1 + U)$ (this was already noted in ref 36).

We propose therefore than in the Mn^{III}–O–Mn^{III} species these additional ferromagnetic contributions occur and that they compete more or less successfully with $J_{yz-yz}{}^{AF}$ (depending on subtle chemical and structural details we do not yet understand).

The strong antiferromagnetism of the Fe^{III}–O–Mn^{III} and Fe^{III}–O–Cr^{III} systems can be understood because compared to Mn^{III}–O–Mn^{III} there is one more AF contribution ($J_{z^2-xz}{}^{AF}$) and fewer ferromagnetic contributions (Figure 10).

Along the same lines the Cr^{III}–O–Cr^{III} and the Cr^{III}–O–Mn^{III} species should be weakly AF or F coupled, which they are. The strong ferromagnetism of the V^{III}–O–V^{III} system would be related to the disappearance, of the $J_{yz-yz}{}^{AF}$ pathway, leaving only ferromagnetic pathways available. This implies that the *xz* orbital is substantially lower in energy than the *yz* which is not immediately obvious. In the following section we present the results of an extended Hückel calculation on a N_5FeO model unit that gives about the same energy for those orbitals but in this calculation only one σ orbital has been included on the N atoms; π effects were not studied. The strong AF of the Ti^{III}–O–Ti^{III} system also poses a problem which we will deal with in a later section.

The previously proposed explanation[9] for the strong antiferromagnetism of the Fe^{III}–O–Fe^{III} system, which is based primarily on the $J_{z^2-z^2}{}^{AF}$ pathway allows one to understand the drop in intensity of the antiferromagnetic coupling in Mn^{III}–O–Mn^{III}, but it does not explain the observed strong AF of Fe^{III}–O–Mn^{III} and Fe^{III}–O–Cr^{III} complexes.

A Refinement of the Model. In the preceding part we focused on the leading orbital interactions. Now we want to examine more

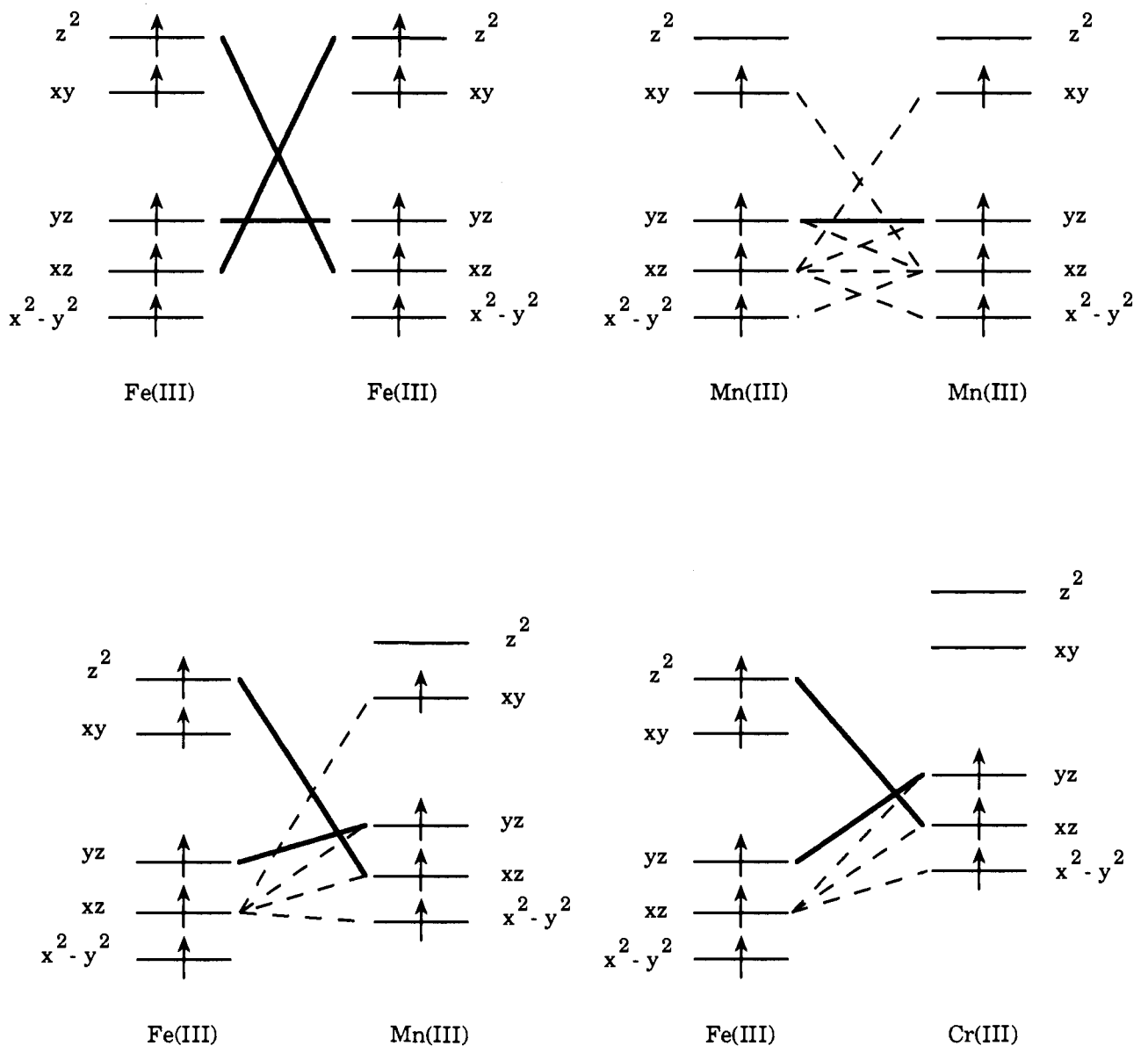

Figure 10. Dominant electron exchange pathways in $[MO(CH_3CO_2)_2M']^{2+}$ units: (i) M = Fe, M′ = Fe; (ii) M = Mn, M′ = Mn; (iii) M = Fe, M′ = Mn; (iv) M = Fe, M′ = Cr. Bold lines symbolize AF couplings while dotted lines stand for F couplings.

quantitatively the overlaps between localized orbitals. In order to achieve this evaluation, we used extended Hückel calculations. In simple cases, an orbital a_i will combine with an orbital b_i to give the two MOs, $(a_i \pm b_i)/\sqrt{2}$ (if one neglects overlap), the energy of which will be $\alpha_i \pm \beta_{ii}$ (again with overlap neglected). The quantity β_{ii} can be estimated from the energies of those MOs. Here the method is slightly more complex since, due to the low symmetry of the complex, a given local orbital can contribute to more than two MOs.

(a) Extended Hückel Calculation for a N_5Fe^{III}–O–$Fe^{III}N_5$ Model. We have calculated the molecular orbitals of a simple model N_5Fe^{III}–O–$Fe^{III}N_5$. The distances around each Fe atom were those of the $[LFe(\mu\text{-}O)(\mu\text{-}CH_3CO_2)_2FeL]^{2+}$ from ref 43. The bridging angle was fixed at 120°, and the nitrogen atoms were modelled by one σ orbital. The results are presented in Figure 11 where the MOs are labeled by the C_{2v} irreducible representations. In the same figure we include the MOs for the N_5Fe^{III}–O fragment. We find the same orbital ordering as in the qualitative scheme proposed above.

Due to the low symmetry of the dinuclear unit, several MOs have the same symmetry label. This complicates the Anderson–Hoffmann approach since the usual transformation $(\phi_u \pm \phi_g)/\sqrt{2}$ is a priori no longer a valid method to obtain orthogonal localized orbitals.

Table XI. Metal d Orbital Composition on Center A of Some of the Metal Rich Molecular Orbitals for the Dinuclear Unit N_5Fe–O–FeN_5 Computed from Eq 19

	z^2 (a_1)	z^2 (b_1)	xy (a_2)	xy (b_2)
d_{z^2}	0.6521	0.6521	0	0
d_{xy}	0	0	0.6753	0.6753
d_{yz}	0	0	0	0
d_{xz}	0	0	0	0
$d_{x^2-y^2}$	0.0478	0.0478	0	0

We propose the following as a solution. The results of the composition of the metal d orbitals for the mononuclear unit are presented in Table X.

Neglecting the overlap integrals we get at first order eq 19

$$z^2(a_1) = (z^2_A + z^2_B)/\sqrt{2}$$
$$z^2(b_1) = (z^2_A - z^2_B)/\sqrt{2}$$
$$xy(a_2) = (xy_A - xy_B)/\sqrt{2} \qquad (19)$$
$$xy(b_2) = (xy_A + xy_B)/\sqrt{2}$$

from which Table XI can be constructed.

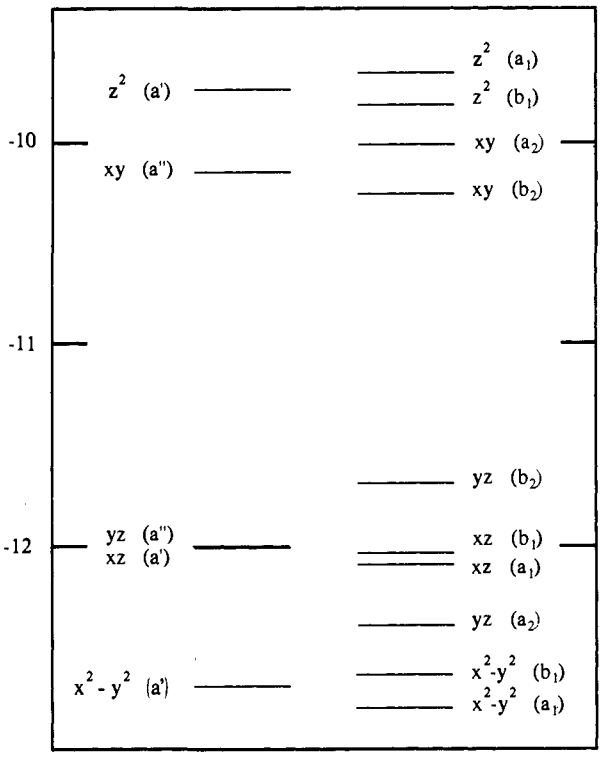

Figure 11. Metal d rich orbitals for the N_5FeO fragment (left-hand side) and the N_5Fe–O–FeN_5 model (Fe–O–Fe angle = 120°) (right-hand side).

Table XII. Metal d Orbital Composition on Center A of Some of the Metal Rich Molecular Orbitals for the Dinuclear Unit N_5Fe–O–FeN_5 Computed by the Extended Hückel Method

	z^2 (a_1)	z^2 (b_1)	xy (a_2)	xy (b_2)
d_{z^2}	0.6475	0.6467	0	0
d_{xy}	0	0	0.6717	0.6773
d_{yz}	0	0	0.0083	0.0134
d_{xz}	0.0680	−0.0952	0	0
$d_{x^2-y^2}$	0.0486	0.0407	0	0

Comparison of the values in Table XI with the values obtained by calculation on the dinuclear unit itself (Table XII) reveals that for the MOs $z^2(a_1)$ and $z^2(b_1)$ the Hückel calculation gives a d_{xz_A} contribution which expresses the z^2–xz interaction mentioned above. There is also a mixing of the $xy(a_2)$ and the $xy(b_2)$ orbitals with the d_{yz_A} orbitals, but this effect is about 10 times smaller.

Is it possible to deduce from this calculation the value of the interaction β_{z^2-xz}? This mixing will have a second-order effect on the energy and a first-order effect on the wave function. We can write eqs 20 and 21

$$z^2(a_1) = \frac{z_A^2 + z_B^2}{\sqrt{2}} + \left[\frac{\beta_{z^2-xz}}{\Delta_{a1}}\right]\frac{xz_A + xz_B}{\sqrt{2}} \qquad (20)$$

$$z^2(b_1) = \frac{z_A^2 - z_B^2}{\sqrt{2}} + \left[-\frac{\beta_{z^2-xz}}{\Delta_{b1}}\right]\frac{xz_A - xz_B}{\sqrt{2}} \qquad (21)$$

where Δ_{a1} is the gap between the MO $z^2(a_1)$ and the MO $xz(a_1)$: Δ_{a1} = 2.43 eV and Δ_{b1} = 2.21 eV. Using coefficients from Table XII one finds β_{z^2-xz} = 0.25 or 0.32 eV. We take an approximate value of 0.30 eV.

The other noncrossed interactions were evaluated from first-order perturbation theory. The values for different interactions are given in Table XIII. Note that the signs of those interactions are dependent on the choice of the phase of the localized orbitals, but it has no physical effect. The convention selected is summarized in Table XIV.

The calculation confirms our previous qualitative ordering of these interactions. The leading ones are the β_{yz-yz} and β_{xz-z^2}. The $\beta_{z^2-z^2}$ term is about four times weaker than the dominant ones.

Table XIII. Orbital Interactions in eV for the N_5Fe–O–FeN_5 Model (Fe–O–Fe Angle = 120°)

z^2/z^2	−0.08	xz/xz	−0.02
xy/xy	0.12	x^2-y^2/x^2-y^2	0.09
yz/yz	**0.35**	**xz/z²**	**0.30**

Table XIV. Sign Convention for the Energy of Each Metal Rich Molecular Orbital for N_5Fe–O–FeN_5 Model

molecular orbital	energy
z^2 (a_1)	$\alpha_{z^2} + \beta_{z^2/z^2}$
z^2 (b_1)	$\alpha_{z^2} - \beta_{z^2/z^2}$
xy (a_2)	$\alpha_{xy} - \beta_{xy/xy}$
xy (b_2)	$\alpha_{xy} + \beta_{xy/xy}$
yz (b_2)	$\alpha_{yz} + \beta_{yz/yz}$
yz (a_2)	$\alpha_{yz} - \beta_{yz/yz}$
xz (b_1)	$\alpha_{xz} - \beta_{xz/xz}$
xz (a_1)	$\alpha_{xz} + \beta_{xz/xz}$
x^2-y^2 (b_1)	$\alpha_{x^2-y^2} - \beta_{x^2-y^2/x^2-y^2}$
x^2-y^2 (a_1)	$\alpha_{x^2-y^2} + \beta_{x^2-y^2/x^2-y^2}$

Table XV. Antiferromagnetic Index (Defined as $I = (1/n_A n_B)\sum_{i,j\ \text{half occupied}} 4\beta_{ij}^2$ in eV² from the N_5Fe–O–FeN_5 Model Calculation[a]

	Ti	V	Cr	Mn	Fe
Ti	0.032		0.011	0.008	
	(0.60)		(0.21)	(0.15)	
V					
Cr			0.058	0.044	0.059
			(1.09)	(0.83)	(1.11)
Mn				0.036	0.047
				(0.68)	(0.89)
Fe					0.053
					(1.00)

[a] In parentheses are the values normalized to the Fe–Fe one.

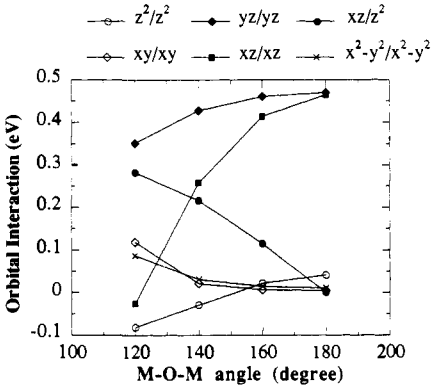

Figure 12. Orbital interactions in the N_5Fe–O–FeN_5 unit for different angles. One can remark: at 120°, the dominant β_{yz-yz} and β_{z^2-xz} pathways; at 180°, the dominant β_{yz-yz} and β_{xz-xz} and the vanished β_{z^2-xz} pathways.

It is clear that we cannot expect to compute the J value from such a simple calculation. In particular the value for the excitation energy U is very difficult to evaluate. Nevertheless, we propose to estimate the antiferromagnetic part of J by computing what one can call the antiferromagnetic index, eq 22.

$$I = \frac{1}{n_A n_B} \sum_{i,j\ \text{half occupied}} 4\beta_{ij}^2 \qquad (22)$$

The results are reported in Table XV. Comparison with Table IX provides some understanding of the magnetic properties of this series. In particular the AF of the Ti^{III}–O–Ti^{III} unit can now be understood: it is due to the $\beta_{x^2-y^2,x^2-y^2}$ interaction, which although small is not negligible and to the factor $n_A n_B$ = 1. One must recognize that this calculation has been made only for Fe and that the more diffuse character of the 3d Ti orbitals would increase the J value compared to the one obtained for Fe–O–Fe.

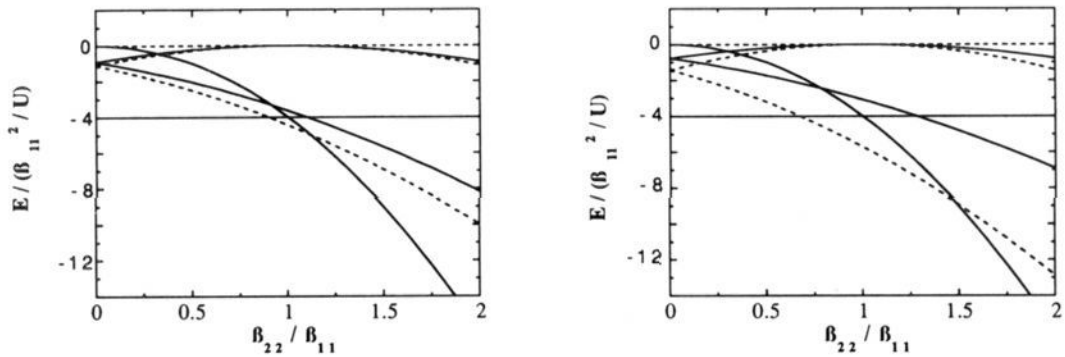

Figure 13. Energy levels in unit of β_{11}^2/U corresponding to two orbitally doubly degenerate states of spin $S = {}^1/_2$ in magnetic interaction as a function of the ratio β_{22}/β_{11}. Left: the local exchange integral K is such that $K/U = 0.1$. Right: the local exchange integral K is such that $K/U = 0.3$: (—) $S = 0$ states and (--) $S = 1$ states.

Calculations were also made on a $N_3Fe(HCO_2)_2FeN_3$ model and did not change the preceding conclusions.

(b) Influence of the Angle. The correlation between the M–O–M angle value and electron counting for the M ion has been studied by Tatsumi and Hoffmann.[44] The influence of the same angle and the torsional angle between mononuclear fragments on the J coupling has been studied theoretically and experimentally in the Fe case by Holm et al.[45] Que et al.[46] recently studied experimentally the influence of the Fe–O–Fe angle on the coupling. We now describe our theoretical results on the influence of the M–O–M angle on the J coupling.

Let us first intuitively guess what the results must be. The S_{yz-yz} overlap is not affected by opening the angle which is confirmed by our calculation. The S_{xz-z^2} overlap is strongly angular dependent since at 180° it has to be zero as evident in the following scheme:

As the S_{xz-z^2} overlap vanishes, the S_{xz-xz} one increases.

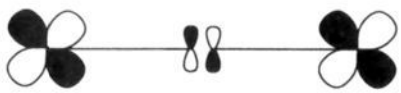

The S_{xy-xy} and $S_{(x^2-y^2)-(x^2-y^2)}$ overlaps decrease when the M–O–M angle opens up, whereas the $S_{z^2-z^2}$ is expected to increase.

These qualitative considerations are fully verified by the calculations, the results of which are reported in Figure 12 which shows the variation of the interaction energy as a function of this angle. The dominant interactions at 180° are the β_{xz-xz} and β_{yz-yz} ones. The $\beta_{z^2-z^2}$ is not as important due to the $2s_O$ participation. At 120° the dominant interactions are the β_{xz-z^2} and the β_{yz-yz} as explained above.

The Fe^{III}–O–Fe^{III} system remains strongly AF whatever the angle because as the $J_{xz-z^2}{}^{AF}$ decreases in absolute value the $J_{xz-xz}{}^{AF}$ increases in absolute value. It is clear that the Mn^{III}–O–Mn^{III} and Cr^{III}–O–Cr^{III} systems must be strongly dependent on the M–O–M angle. This appears to be the case. In contrast to the $[Mn^{III}(\mu\text{-}O)(\mu\text{-}CH_3CO_2)_2Mn^{III}]^{2+}$ systems, a linear Mn^{III}–O–Mn^{III} unit is strongly AF coupled ($J = -240$ cm^{-1} in ref 39). A $[Cr^{III}(\mu\text{-}O)(\mu\text{-}CH_3CO_2)Cr^{III}]^{3+}$ unit has recently been found to be AF coupled[40] with $J = -100$ cm^{-1}. For the linear $[(NH_3)_5Cr^{III}\text{–}O\text{–}Cr^{III}(NH_3)_5]^{4+}$ complex $J = -450$ cm^{-1}.[47] The V^{III}–O–V^{III} could be AF if the local configuration is $(x^2\text{–}y^2)^1(xz)^1$, but this case can be complicated (see below). Complexes containing a linear Ti^{III}–O–Ti^{III} moiety should be paramagnetic as has been reported for $[L'_2Ti_2Cl_4(\mu\text{-}O)]$.[17] So the Ti^{III}–O–Ti^{III} coupling is very sensitive to the Ti–O–Ti angle.

(c) The V^{III}–O–V^{III} Ferromagnetism. A puzzling result related to this study is the ferromagnetic coupling observed in bent and linear V^{III}–O–V^{III} systems.[18a,b]

We have suggested above that the ferromagnetic coupling of the $[V^{III}(\mu\text{-}O)(\mu\text{-}CH_3CO_2)_2V^{III}]^{2+}$ complex is related to the crossed pathway. This implies that the xz orbital is lower in energy than the yz one, which remains to be checked experimentally.

Such a mechanism cannot be valid for a linear V^{III}–O–V^{III} system which is also found to be ferromagnetically coupled. In this system the interaction energy β_{yz-yz} and β_{xz-xz} must be very similar and the β_{xz-z^2} interaction has to be zero by symmetry. One way to rationalize the ferromagnetic coupling is to use the MO scheme in the following way:

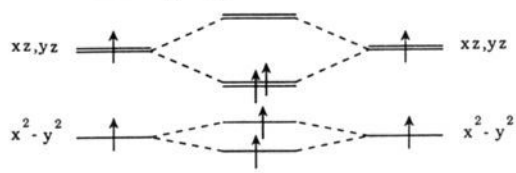

In fact the symmetry is not exactly D_{4h}, and the strict degeneracy of the highest singly occupied MOs orbitals is not guaranteed. A gap could exist which could be large enough to give a low-spin species as for $Cu_2(CH_3CO_2)_4{\cdot}2H_2O$ for instance. In fact we show in the Appendix that due to orbital degeneracy the situation is quite different from that for $Cu_2(CH_3CO_2)_4{\cdot}2H_2O$ and that the triplet is stabilized even when the degeneracy of the two MOs is not realized.

Let us consider the simplified case of two electrons on two centers, each center presenting two degenerate orbitals:

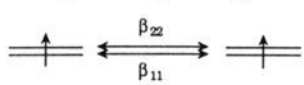

We found the following states and energies (see Appendix): four spin triplet states at the energies 0 (doubly degenerate) and $-(\beta_{11} \pm \beta_{22})^2/(U\text{–}K)$ and four singlet states at the energies $-4\beta_{11}{}^2/U$, $-4\beta_{22}{}^2/U$, and $-(\beta_{11} \pm \beta_{22})^2/(U + K)$. If $\beta_{11} = \beta_{22} = \beta$, the ground state is a spin triplet state (as predicted by simple MO theory) at $-4\beta^2/(U - K)$, and the first excited states are singlet

(39) Kipke, C. A.; Scott, M. J.; Gohdes, J. W.; Armstrong, W. *Inorg. Chem.* **1990**, *29*, 2193–2194.
(40) Gafford, B. G.; Marsh, R. E.; Schaefer, W. P.; Zhang, J. H.; O'Connor, C. J.; Holwerda, R. A. *Inorg. Chem.* **1990**, *29*, 4652–4657.
(41) Weaver, T. R.; Meyer, T. J.; Adeyemi, S. A.; Brown, G. M.; Eckberg, R. P.; Hatfield, W. E.; Johnson, E. C.; Murray, R. W.; Untereker, D. *J. Am. Chem. Soc.* **1975**, *97*, 3039–3048.
(42) Phelps, D. W.; Kahn, E. M.; Hodgson, D. J. *Inorg. Chem.* **1975**, *14*, 2486–2490.
(43) Spool, A.; Williams, I. D.; Lippard, S. J. *Inorg. Chem.* **1985**, *24*, 2158.
(44) Tatsumi, K.; Hoffmann, R. *J. Am. Chem. Soc.* **1981**, *103*, 3328–3341.
(45) Mukherjee, R. N.; Stack, T. D. P.; Holm, R. H. *J. Am. Chem. Soc.* **1988**, *110*, 1850–1861.
(46) Norman, R. E.; Holz, R. C.; Ménage, S.; Que, L., Jr.; Zhang, J. H.; O'Connor, C. J. *Inorg. Chem.* **1990**, *29*, 4629–4637.
(47) Güdel, H. U.; Dubicki, L. *Chem. Phys.* **1974**, *6*, 272.

spin states at $-4\beta^2/U$. The gap is of the form $4\beta^2K/U^2$. If β_{11} is not equal to β_{22} it is still possible to have a spin triplet ground state. This will depend on the parameters. This is illustrated in Figure 13 which shows the energies of the lowest states as a function of the ratio β_{22}/β_{11}. Figure 13 (left) corresponds to a low local exchange integral K (diffuse d orbitals) and Figure 13 (right) to a high local exchange integral K (contracted d orbitals). If K is large, the system will maintain a spin triplet ground state even with a substantial difference between the β_{ii} interactions. The opposite is true if K is small.

This is reminiscent of the problem concerning the electronic properties of $[L_5Ru^{III}-O-Ru^{III}L_5]^{n+}$ complexes. A singlet spin ground state has been observed with a triplet spin first excited state[41] at 170 cm^{-1}. Meyer et al. suggested that this is due to a gap between the two highest occupied MOs without going into the preceding details. This gap was related to asymmetry in the coordination and bending of the Ru–O–Ru unit.

Our calculation could suggest that such a molecule would have a spin triplet ground state in contradiction with the experiment. Nevertheless, due to the diffuse nature of the 4d orbitals, the local exchange integral K is smaller than for 3d orbitals, and the Ru–O–Ru angle (157.2°)[42] is sensibly distinct from 180°. Those two factors destabilize the triplet state (Figure 13 (left)) and could explain, even in our model, the observation of a singlet ground state.

Conclusion

We would like to summarize the main results of this study.

(i) Heterodinuclear $[M(\mu\text{-}O)(\mu\text{-}CH_3CO_2)_2M']^{n+}$ complexes have been prepared, and their magnetic behavior has been found to be highly diverse depending on the d^n-electron configuration of M and M′.

(ii) We have identified the S_{xz-z^2} and S_{yz-yz} overlaps as the leading ones. This can be intuitively understood and has been checked by extended Hückel calculations.

(iii) The *same interaction* between orbitals xz and z^2 has been suggested as the origin of strong antiferromagnetic coupling when the orbitals are half-occupied or ferromagnetic coupling when the z^2 orbital is empty and the xz orbital is half-occupied.

(iv) The angular dependence of the coupling constant J can be rationalized mainly through the variations of the xz–z^2, xz–xz, and yz–yz interactions. The Fe^{III}–O–Fe^{III} J values are practically independent of the angle. These orbital interactions can rationalize why even when the Mn^{III}–O–Mn^{III} and Cr^{III}–O–Cr^{III} angle increases the AF couplings increase. In contrast, the Ti^{III}–O–Ti^{III} complexes become less AF when the angle increases.

(v) The ferromagnetic behavior of the bent and linear V^{III}–O–V^{III} is much more difficult to understand. We suggest that in the bent case the highest half-occupied ligand field orbital is the xz one; in that case the main orbital interaction is the xz–z^2 one which leads to ferromagnetic coupling. In the linear case we stressed the orbitally degenerate character of the local V^{III} state, and we showed that this can also lead to ferromagnetic coupling.

Appendix

We present here some indications about the calculation of the states and their energy for a dinuclear unit with two unpaired electrons and two degenerate orbitals a_1 and a_2 on A and b_1 and b_2 on B. We have four homopolar configurations: a_1b_1, a_1b_2, a_2b_1, a_2b_2 and six heteropolar configurations a_1^2, a_2^2, a_1a_2, b_1^2, b_2^2, b_1b_2. The latter generate six spin singlet states and two triplet states. The homopolar configurations generate four triplet states and four singlet states. We parametrized the energies with β_{11} and β_{22}, U for the electron–electron repulsion on site A or B and K for the local exchange integral. For noninteracting sites, the homopolar states are degenerate. The heteropolar singlet states built on configurations a_1^2, a_2^2, b_1^2, b_2^2 are at the energy U and those derived from configurations a_1a_2 and b_1b_2 are at the energy $U + K$. The heteropolar triplet states are at the energy $U - K$. Interactions β_{11} and β_{22} between sites A and B lift this degeneracy through mixing with the heteropolar states, and we are interested in the final states.

The matrix of interaction for the ten singlet states is easy to build as is the one for the six triplet states. Using second-order perturbation theory it is easy to derive from those matrices the expression given in the text.

Acknowledgment. This work was supported by the Deutsche Forschungsgemeinschaft and the Fonds der Chemischen Industrie. We thank both institutions.

Supplementary Material Available: Lists of bond distances, bond angles, anisotropic displacement parameters, and calculated positional parameters for hydrogen atoms for complexes **3**, **4**, **5**, and **6** (18 pages); listings of observed and calculated structure amplitudes (90 pages). Ordering information is given on any current masthead page.

(48) Martin, L. L.; Wieghardt, K.; Blondin, G.; Girerd, J. J.; Nuber, B.; Weiss, J. *J. Chem. Soc., Chem. Commun.* **1990**, 1767.
(49) Sanders-Loehr, J.; Wheeler, W. D.; Shiemke, A. K.; Averill, B. A.; Loehr, T. M. *J. Am. Chem. Soc.* **1989**, *111*, 8084–8093.
(50) McCarthy, P. J.; Güdel, H. U. *Coord. Chem. Rev.* **1988**, *88*, 69–131.